AD-A127 135 APPLICATIONS OF JOSEPHSON JUNCTION SQUIDS (SUPERCONDUCTING QUANTUM INTERF..(U) TRW SPACE AND TECHNOLOGY GROUP REDONDO BEACH CA APPLIED TECHN.. 1/1

UNCLASSIFIED A H SILVER NOV 82 N00014-81-C-0615 F/G 9/5 NL

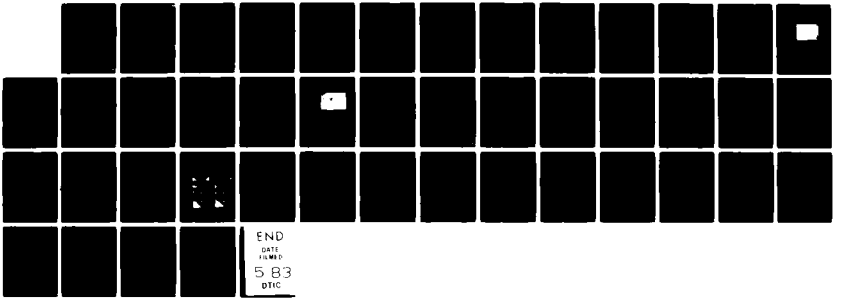

END
DATE FILMED
5 83
DTIC

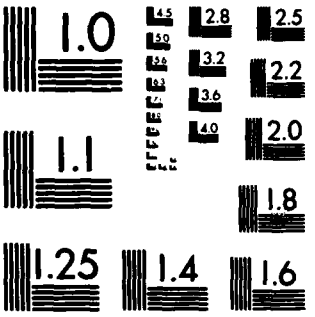

MICROCOPY RESOLUTION TEST CHART
NATIONAL BUREAU OF STANDARDS-1963-A

TRW Space & Technology Group
One Space Park
Redondo Beach, CA 90278
213 535 4321

12

TRW

AD A127135

ANNUAL REPORT

TO THE

OFFICE OF NAVAL RESEARCH
CODE 414
800 N. QUINCY ST.
ARLINGTON, VA 22217

ON

APPLICATIONS OF JOSEPHSON JUNCTION SQUIDS AND ARRAYS

CONTRACT NO. N00014-81-C-0615

SEPTEMBER 1981 - SEPTEMBER 1982

PREPARED BY

A.H. SILVER
ADVANCED PRODUCTS LABORATORY
APPLIED TECHNOLOGY DIVISION
TRW

DTIC ELECTE
APR 22 1983
A

NOVEMBER 1982

DTIC FILE COPY

This document has been approved for public release and sale; its distribution is unlimited.

88 04 21 136

TRW Inc.
Electronics &
Defense Sector

One Space Park
Redondo Beach, CA 90278
213.535.4321

ANNUAL REPORT

TO THE

OFFICE OF NAVAL RESEARCH
CODE 414
800 N. QUINCY ST.
ARLINGTON, VA 22217

ON

APPLICATIONS OF JOSEPHSON JUNCTION SQUIDS AND ARRAYS

CONTRACT NO. N00014-81-C-0615

SEPTEMBER 1981 - SEPTEMBER 1982

PREPARED BY

A.H. SILVER
ADVANCED PRODUCTS LABORATORY
APPLIED TECHNOLOGY DIVISION
TRW

NOVEMBER 1982

Accession For
GRA&I
TAB
Dist
A

UNCLASSIFIED

SECURITY CLASSIFICATION OF THIS PAGE (When Data Entered)

REPORT DOCUMENTATION PAGE		READ INSTRUCTIONS BEFORE COMPLETING FORM
1. REPORT NUMBER	2. GOVT ACCESSION NO. AD-A127135	3. RECIPIENT'S CATALOG NUMBER
4. TITLE (and Subtitle) Applications of Josephson Junction SQUIDs and Arrays		5. TYPE OF REPORT & PERIOD COVERED Annual Progress Report September 1981 - September'82
		6. PERFORMING ORG. REPORT NUMBER
7. AUTHOR(s) A. H. Silver		8. CONTRACT OR GRANT NUMBER(s) N00014-81-C-0615
9. PERFORMING ORGANIZATION NAME AND ADDRESS Advanced Products Laboratory TRW Space and Technology Group One Space Park, Redondo Beach, CA 90278		10. PROGRAM ELEMENT, PROJECT, TASK AREA & WORK UNIT NUMBERS P.E. 61153N
11. CONTROLLING OFFICE NAME AND ADDRESS Office of Naval Research Code 414 800 N. Quincy St. Arlington, VA 22217		12. REPORT DATE November 1982
		13. NUMBER OF PAGES 41
14. MONITORING AGENCY NAME & ADDRESS(if different from Controlling Office)		15. SECURITY CLASS. (of this report) Unclassified
		15a. DECLASSIFICATION/DOWNGRADING SCHEDULE N/A

16. DISTRIBUTION STATEMENT (of this Report)

Approved for Public Release
Unlimited Distribution

17. DISTRIBUTION STATEMENT (of the abstract entered in Block 20, if different from Report)

18. SUPPLEMENTARY NOTES

19. KEY WORDS (Continue on reverse side if necessary and identify by block number)

Josephson Junctions, SQUIDs, Arrays, Voltage-Controlled-Oscillator, Microwave Oscillator, monolithic superconducting transformers.

20. ABSTRACT (Continue on reverse side if necessary and identify by block number)

This is the first Annual Report for an effort to demonstrate the application of SQUIDs (Superconducting QUantum Interference Device) and SQUID arrays to microwave systems. The application considered here is a microwave voltage-controlled oscillator. We report on the circuit design, numerical simulation, experimental design, and fabrication of the device including tests of the monolithic impedance transformer. Predicted available power is approximately 10 nW into a load impedance of 1Ω ohm.

DD FORM 1 JAN 73 1473 EDITION OF 1 NOV 65 IS OBSOLETE

UNCLASSIFIED

SECURITY CLASSIFICATION OF THIS PAGE (When Data Entered)

TABLE OF CONTENTS

LIST OF FIGURES

I. INTRODUCTION

This is the Annual Progress Report for Contract No. N00014-81-C-0615, "Application of Josephson Junction SQUIDs and Arrays." covering the period from 1 September 1981 through 30 September 1982. The objectives of this program are to define and demonstrate applications of SQUIDs and SQUID arrays via analysis and experiment. The goals of this contract were to investigate and demonstrate the properties of a SQUID voltage-controlled-oscillator (VCO). These goals were met by 1) analysis and simulation of a voltage-clamped resistive SQUID and a voltage-clamped dc SQUID, 2) design, fabrication and measurement of appropriate microwave matching transformer, and, 3) design, fabrication, and measurement of a SQUID VCO. We report on progress in these three areas.

2. WORK PLAN

This is a new contract for a projected multi-year investigation of Superconducting QUantum Interference Device (SQUID) arrays and their application to microwave and gigabit technology. The focus of this contract is the investigation and demonstration of a SQUID voltage-controlled oscillator (VCO). The array is then projected to increase the available power and operating impedance. The approach utilizes monolithic superconducting integrated circuits which were designed, fabricated, and tested at TRW.

Three tasks were undertaken in the first year:

Task 1. Analysis of dc SQUID Arrays

Task 2. Design of dc SQUID Generator

Task 3. SQUID VCO Fabrication and Measurement.

A number of the steps are very similar to those required for a contract with the Naval Research Laboratory, "Demonstration of a SQUID Parametric Amplifier." Such steps were carried out jointly and are reported to both agencies. TRW is concurrently conducting Independent Research and Development on Advanced Josephson Devices. This project is principally concerned with development of a Josephson integrated circuit fabrication capability. Some of the activities of that program which impact this contract are discussed here.

3. PROGRESS

3.1 Transformer Design

Since the SQUID VCO is necessarily a very low impedance device, a suitable transformer is an essential ingredient for evaluating the basic VCO, particularly with respect to available power. In order to carry out this transformation in both impedance and dimension in a reproducible and predictable manner, the transformer is integrated with the active circuitry.

The basic architecture of the transformer was presented in the contract proposal. We have refined the design for the TRW fabrication process and reconsidered the problems of launching from 50Ω coaxial cable into 50Ω coplanar line, dimensional step from 1 mm coplanar line at 50Ω, and construction of capacitors in the lumped element impedance transformer. The electrical design was optimized numerically using COMPACT with a computed VSWR < 1.25 over the 8-12 GHz band (Figure 1). Figure 2 shows the equivalent electrical circuit and the geometrical layout.

A test of the effect of changing dimensions in 50Ω coplanar line was performed by fabricating three 50Ω transmission lines: a continuous coplanar line at mm dimensions, a sharply stepped coplanar line, and a short, tapered transition as shown in Figure 3. The measured performance showed no significant differences between the three lines. Therefore, the input LC circuit in the transformer intended to tune out the inductance of the step in the coplanar line was deleted.

The transformer was designed to be fabricated on a 2 inch silicon wafer, 0.015 in. thick, with a minimum line width of 50μm. An OSM microwave launcher drives the 50Ω coplanar line which has a center conductor width of 50μm, ground plance spacing of 30μm, and an effective dielectric

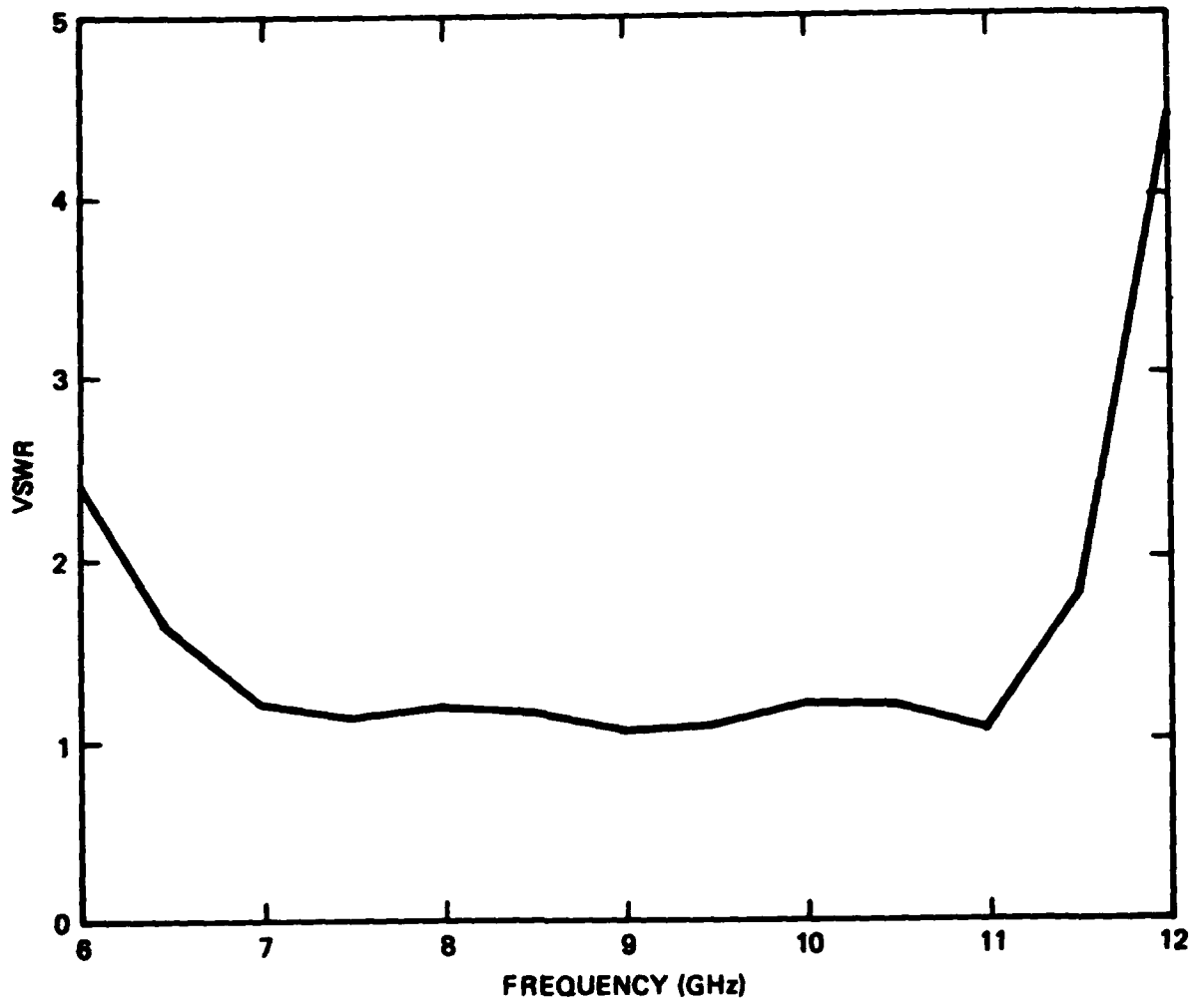

FIGURE 1. Computed voltage standing wave radio (VSWR) as a function of frequency for transformer circuit shown in Figure 3.

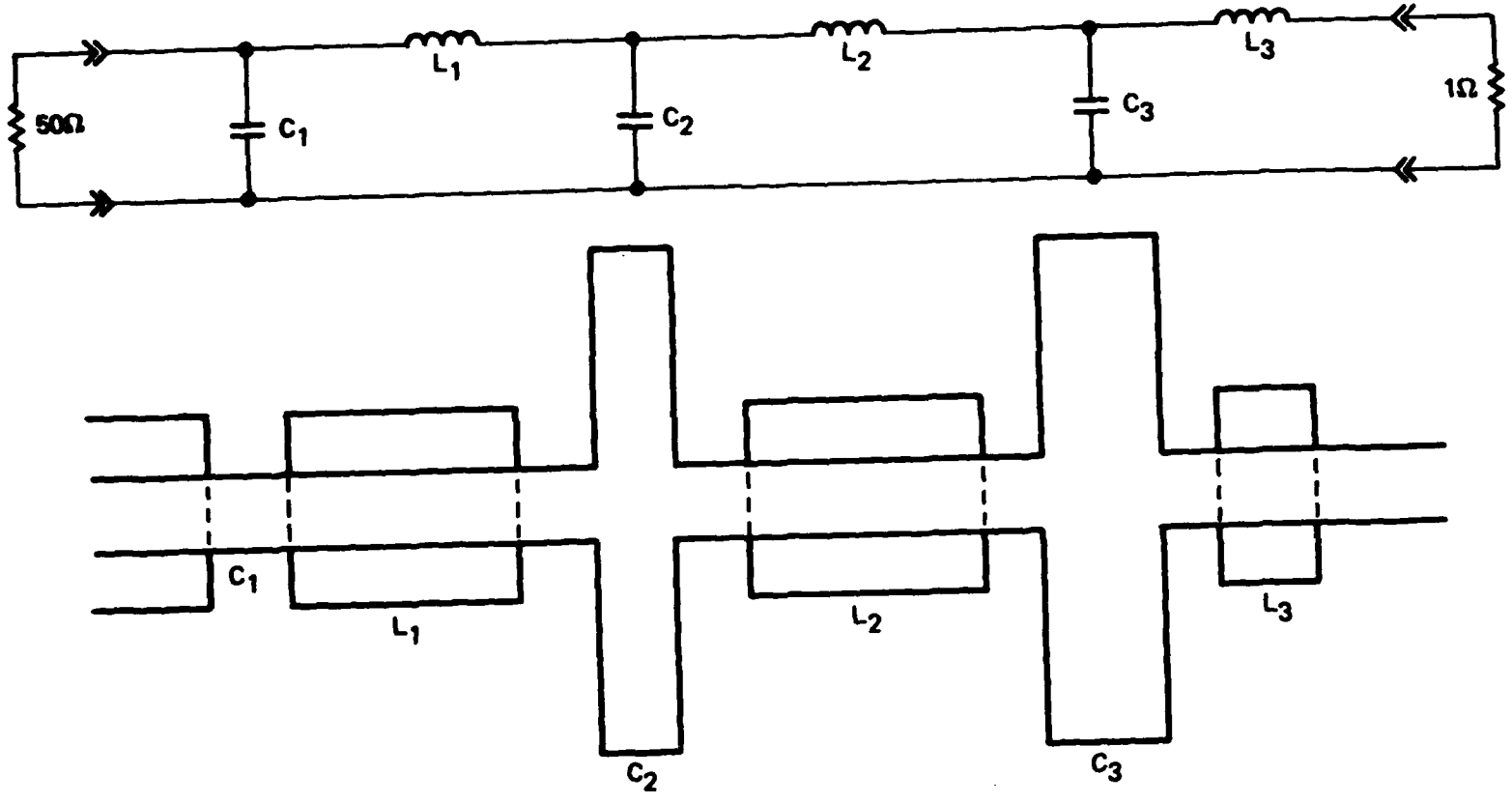

Figure 2. Equivalent circuit (top) and physical layout (not to scale) of X-band transformer designed and simulated. The lumped circuit parameters are C_1 = 0.6 pF, L_1 = 442 pH, C_2 = 1.6 pF, L_2 = 108 pH, C_3 = 8.6 pF, L_3 = 22 pH.

Figure 3. Photograph of the 50Ω coplanar lines used to test dimensional changes.

constant of 6.4. The reduction in ε and its dependence on linewidth results from the finite thickness of the Si substrate. The 1Ω microstrip in the transformer is 50μm wide and separated from the Nb ground plane by 50nm Nb_2O_5 and 200nm SiO. It has an effective ε=13.

The transformer design incorporates short ($< \lambda/4$) sections of coplanar and microstrip lines which act as lumped inductors and capacitors, respectively. The inductive lines are 50Ω coplanar lines terminated by 1Ω microstrip, with $L \simeq Z_o \ell / V$, where Z_o is the line impedance, ℓ the line length, and v the propagation velocity. Capacitors are 1Ω and 0.5Ω microstrip either terminated by 50Ω coplanar or used as open parallel stubs. The capacitance of short, open lines is given by $C \simeq \ell / Z_o v$.

Photolithographic patterns were defined as 4-level masks and produced at the TRW Microelectronics Center for the combined dimensional and impedance transformer. For the dimensions and tolerances required, masks were fabricated directly at the reticle level in an Electromask pattern generator. Figure 4 shows the computer-generated composite of three 1 cm x 2 cm chips which were fabricated on 2" silicon wafers, .015" thick. Each chip has 2 coplanar inputs with tapered lines. On one chip the reduced width coplanar line couples directly through; on the second chip, the transformers from each end are connected for in-out transmission measurements. The third chip has each coplanar line and transformer terminated with a matched resistive load. Figure 5 is an expanded plot of the transformer and terminating resistor on the third chip.

The transformers were fabricated in a 1 cm x 2 cm format on 2" diameter silicon wafers with an insulating SiO_2 surface. Three test chips are produced on each wafer. Following fabrication, the wafers were cleaved with a modified Tempress scriber and the chips mounted in a holder suitable for connection to an OSM coaxial bulkhead launcher. Measurements are made at T=4K with an HP-8410 Network Analyzer. The data are in the form of the scattering matrix coefficients S_{11} and S_{12}. Only the magnitude of S is reported since the phase is difficult to calibrate with long coaxial lines into the helium dewar.

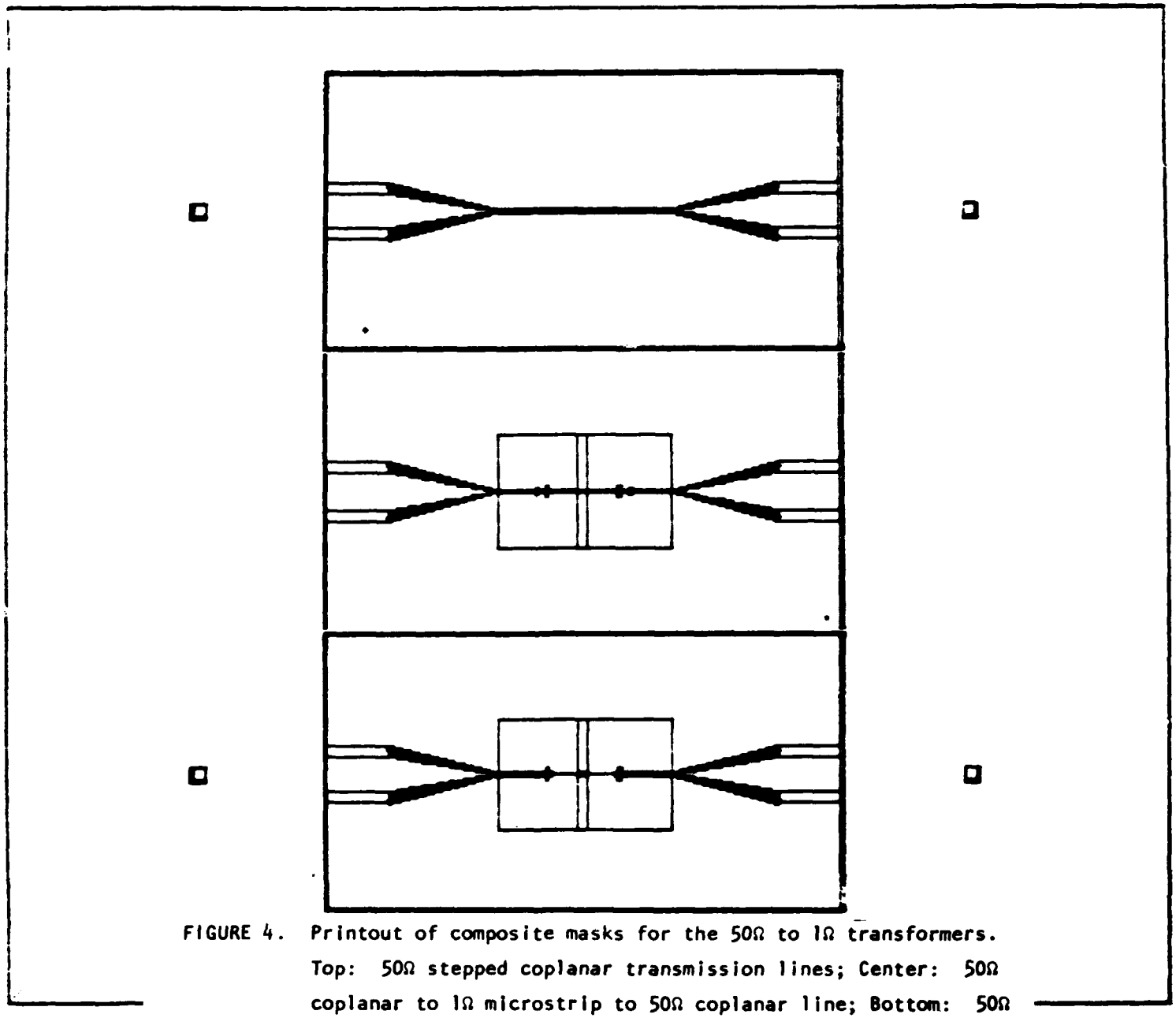

FIGURE 4. Printout of composite masks for the 50Ω to 1Ω transformers. Top: 50Ω stepped coplanar transmission lines; Center: 50Ω coplanar to 1Ω microstrip to 50Ω coplanar line; Bottom: 50Ω coplanar to 1Ω microstrip terminated.

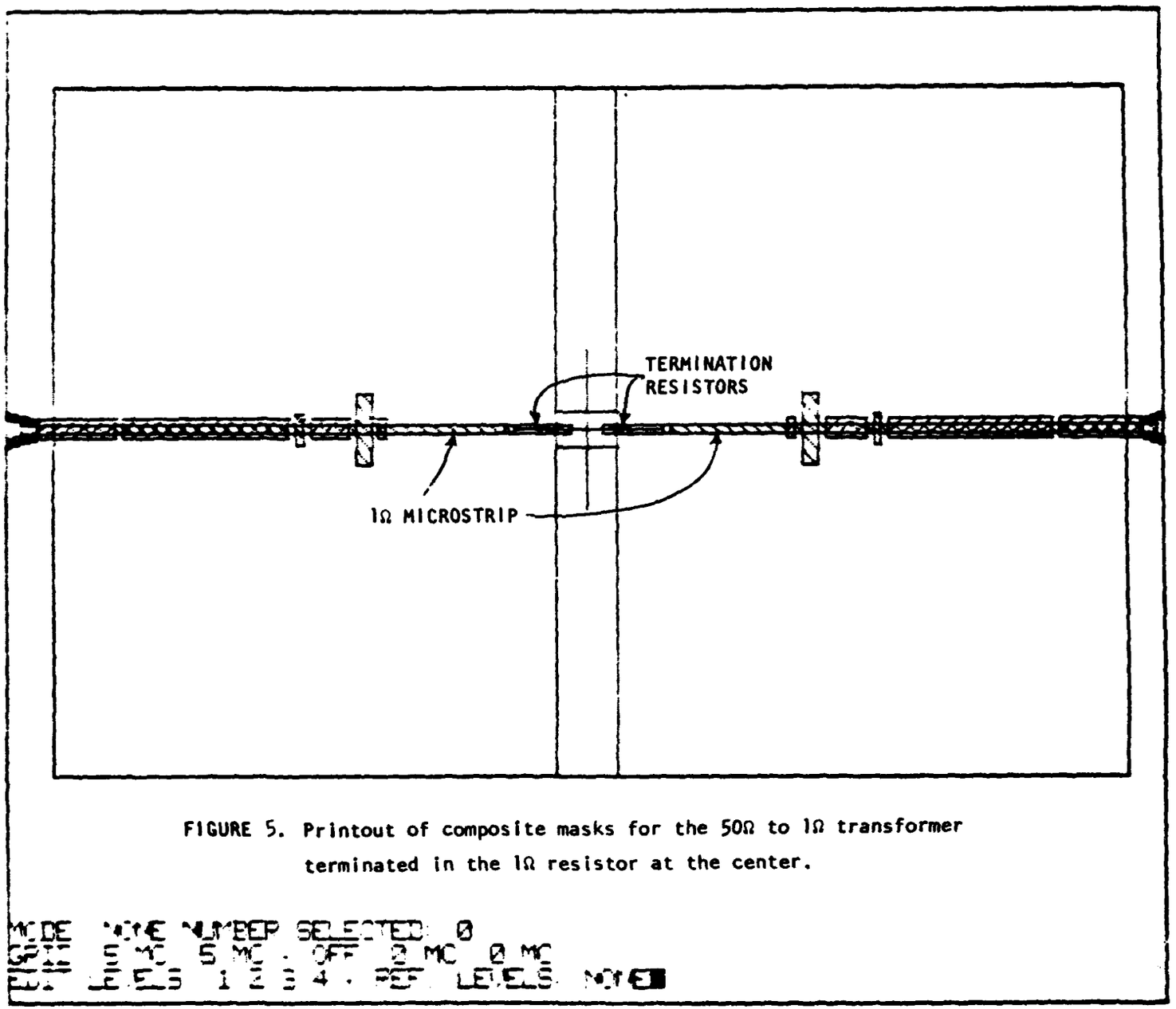

FIGURE 5. Printout of composite masks for the 50Ω to 1Ω transformer terminated in the 1Ω resistor at the center.

The test transformer chips are mounted with a coaxial connector at each end as shown in Figure 6. As anticipated, connecting the coplanar input to the bulkhead connector was a significant problem. An acceptable solution is to use In solder to connect gold ribbon from the connector centerpin and bulkhead to the coplanar lines. To facilitate soldering to the Nb film, a gold film is evaporated over the Nb. This is done before the Nb is patterned. Figure 7 shows the response of the simple tapered coplanar lines at 4 kelvin; Figure 8 the response of the double-ended transformer, in which the 50Ω coplanar line is transformed to 1Ω microstrip at the center of the chip, and then transformed back to 50Ω coplanar at the other end of the chip. We have not measured good S-parameter characteristics with the terminated transformers and we attribute this to a problem in making good contact with the resistors.

3.2 Analysis of Voltage-Clamped SQUIDs

We have investigated the voltage-clamped SQUID in two forms appropriate to the voltage-controlled oscillators, the resistive SQUID of Figure 9 and the dual resistive SQUID with common voltage-biasing resistor which we call the voltage clamped dc SQUID (Figure 10). To the best of our knowledge, neither of these devices incorporating the RSJ model with appropriate capacitance has been fully investigated and thus computer simulation was undertaken to predict the operating characteristics and parameterize the performance.

Analyses were performed with numerical simulations for preselected ranges of the device parameters. Computations of the transient response and subsequent Fourier spectra were performed on a Cyber 174/750 machine. The results are described in a paper which will be given at the 1982 Applied Superconductivity Conference and submitted for publication in the Conference Proceedings to appear in the IEEE Transactions on Magnetics in 1983. The manuscript, "SQUID Voltage-Controlled-Oscillator," is attached as a part of this report. (Appendix A).

The test transformer chips are mounted with a coaxial connector at each end as shown in Figure 6. As anticipated, connecting the coplanar input to the bulkhead connector was a significant problem. An acceptable solution is to use In solder to connect gold ribbon from the connector centerpin and bulkhead to the coplanar lines. To facilitate soldering to the Nb film, a gold film is evaporated over the Nb. This is done before the Nb is patterned. Figure 7 shows the response of the simple tapered coplanar lines at 4 kelvin; Figure 8 the response of the double-ended transformer, in which the 50Ω coplanar line is transformed to 1Ω microstrip at the center of the chip, and then transformed back to 50Ω coplanar at the other end of the chip. We have not measured good S-parameter characteristics with the terminated transformers and we attribute this to a problem in making good contact with the resistors.

3.2 Analysis of Voltage-Clamped SQUIDs

We have investigated the voltage-clamped SQUID in two forms appropriate to the voltage-controlled oscillators, the resistive SQUID of Figure 9 and the dual resistive SQUID with common voltage-biasing resistor which we call the voltage clamped dc SQUID (Figure 10). To the best of our knowledge, neither of these devices incorporating the RSJ model with appropriate capacitance has been fully investigated and thus computer simulation was undertaken to predict the operating characteristics and parameterize the performance.

Analyses were performed with numerical simulations for preselected ranges of the device parameters. Computations of the transient response and subsequent Fourier spectra were performed on a Cyber 174/750 machine. The results are described in a paper which will be given at the 1982 Applied Superconductivity Conference and submitted for publication in the Conference Proceedings to appear in the IEEE Transactions on Magnetics in 1983. The manuscript, "SQUID Voltage-Controlled-Oscillator," is attached as a part of this report. (Appendix A).

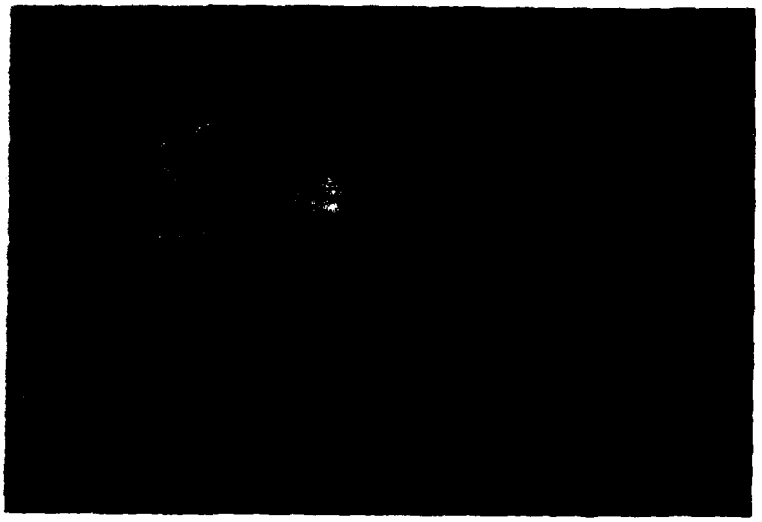

FIGURE 6. Photograph of transformer test chip mounted in a brass holder and connected to two OSM bulkhead connectors. The tapered coplanar lines at each end are visible in the photograph. The grey rectangle in the center of the chip is anodized Nb covered with SiO. The transformers are located in the same rectangle but are not clearly visible in the photograph.

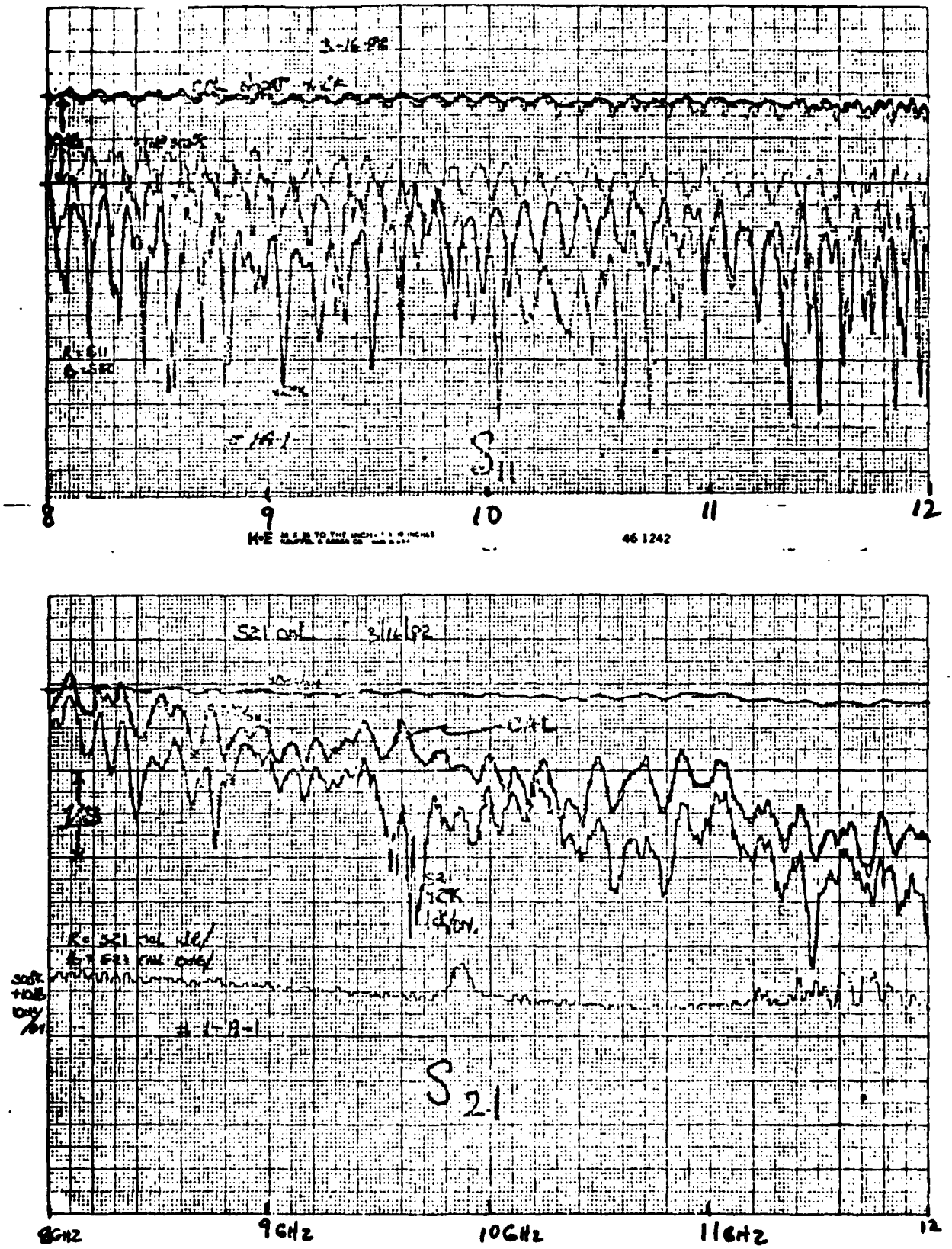

Figure 7. Response of 50Ω tapered coaxial lines on silicon substrate measured at 4K. The upper graph shows S_{11} (and S_{22}) at 4K; the faint curve is S_{11} at 300K. The lower graph is S_{21} at 4K.

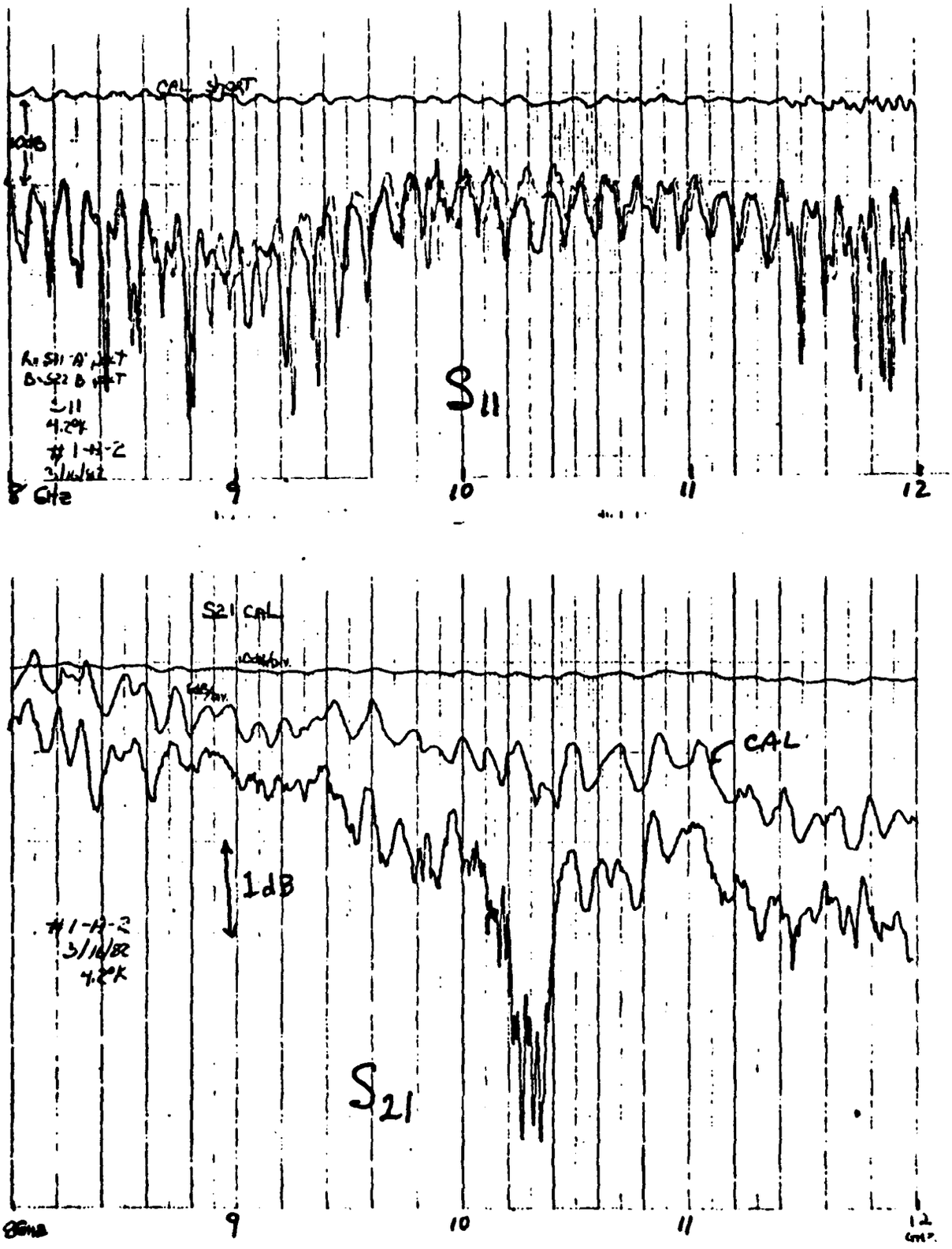

Figure 8. Response of the double-ended 50Ω to 1Ω transformers measured at 4K. The upper graph is S_{11} (and S_{22}), the lower is S_{21}.

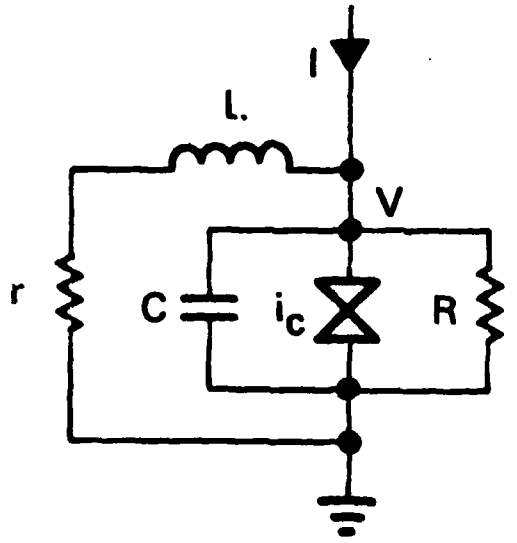

Figure 9. Resistive SQUID VCO. L is the SQUID inductance and r the small voltage-biasing resistor. R is the load resistance which sets the damping.

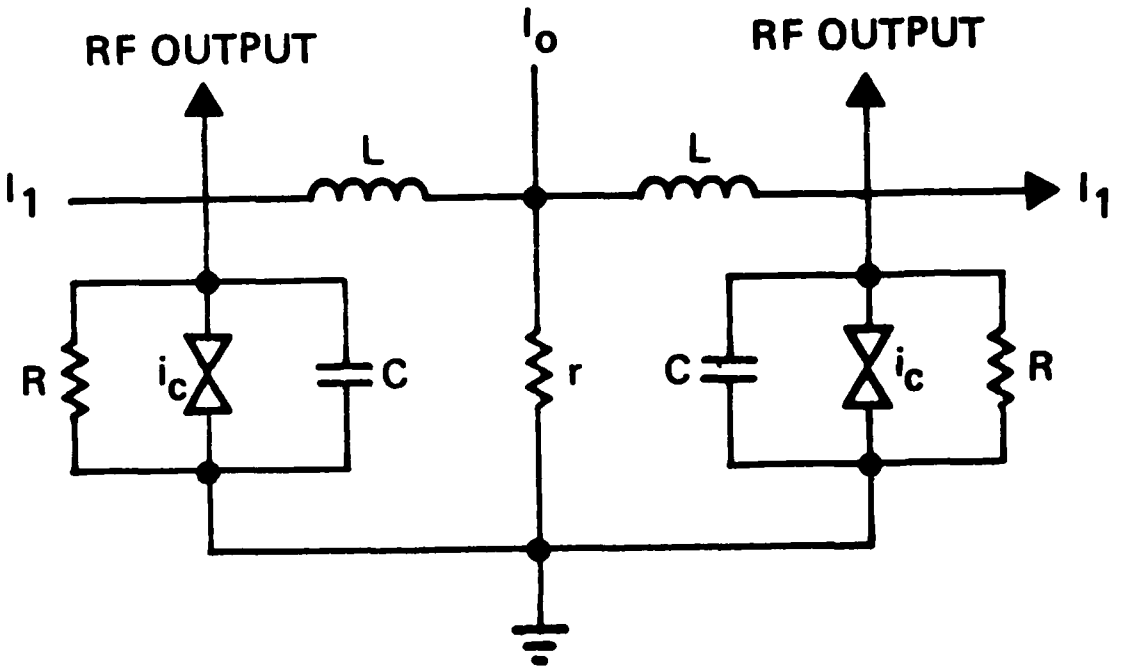

Figure 10. Voltage-clamped dc SQUID. The voltage-clamping resistor is r, and the load resistance is 2R.

3.3 SQUID VCO

3.3.1 Design

The VCO design placed the resistive SQUID at the low impedance end of the 50Ω to 1Ω transformer discussed above. Connection to the transformer is with 1Ω superconducting microstripline. Two devices are placed on each 1 cm x 2 cm chip; four chips are designed on each wafer. The SQUID was designed to utilize the $Nb/Nb_2O_5/PbBi$ junctions in use at TRW, with PbIn interconnecting lines. Figure 11 shows the composite artwork for the VCO wafer. The structures at the top and bottom of each chip are test junctions and resistors.

The impedance of the SQUID, $\sqrt{L/C}$, is set at 0.3Ω, such that the loading of the 1Ω transformer will result in Q≈3.3. Design values are chosen to maximize $\phi_o^2/2L \approx 10^4 kT$ and set β=1, the SQUID resonance frequency equal to 9GHz, and the Josephson plasma resonance frequency also equal to 9GHz. Thus $L = 5pH$

$C = 65pF$

$i_c = 67\mu A$

$j_o = 9A/cm^2$

and the junction area is 50μm x 14.9μm = $745\mu m^2$. The biasing resistance r is independently set with a design value near $10^{-3}\Omega$. This design assumes that the 1Ω load dominates over the internal quasiparticle resistance.

Because of the nature of the response for Q>2, we varied the design for each of the four chips on the wafer as follows:

VCO #	L(pH)	C(pF)	Q	$i_c(\mu A)$	$R_d(\Omega)$
1	5	65	3.3	67	---
2	10	32.5	1.7	33.5	---
3	5	65	1.7	67	1
4	2.5	130	1.7	134	0.25

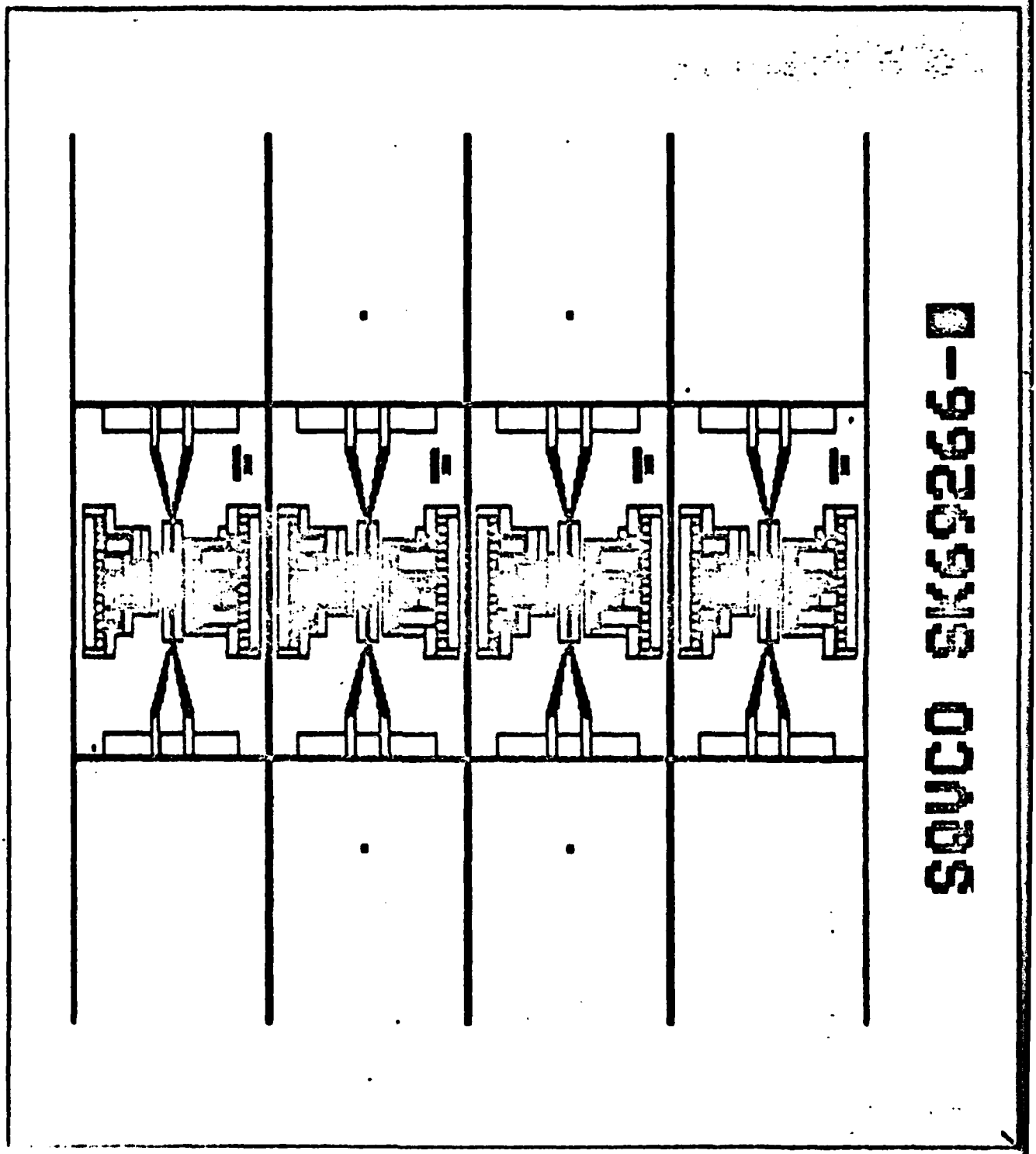

Figure 11a. Composite of seven masks designed for the four VCO circuits. Test junctions and resistors are placed above and below each of the 2 VCO's per chip.

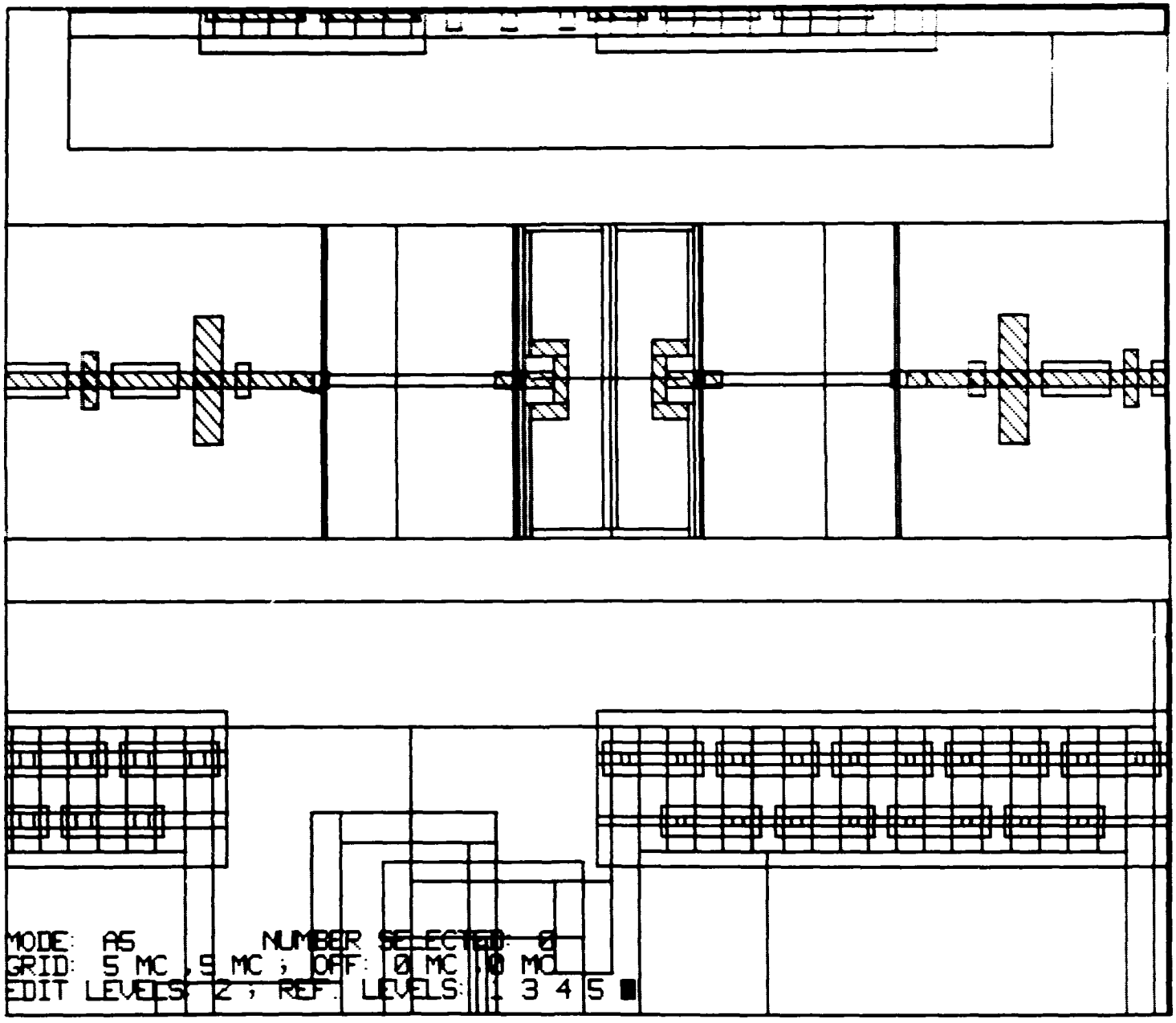

Figure 11b. Composite of mask artwork for the central section of VCO #2.

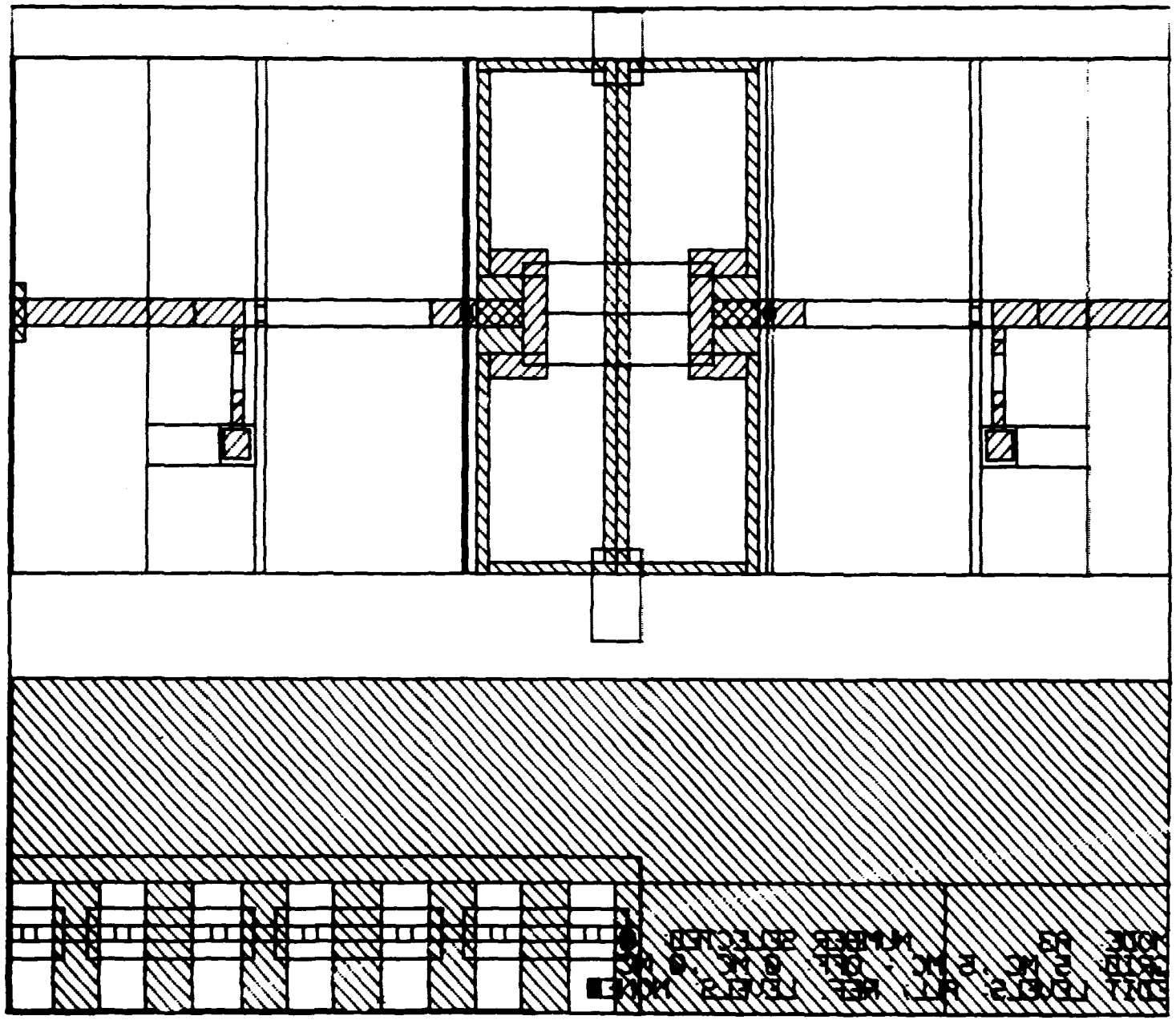

Figure 11c. Composite of mask artwork for the central section of VCO #3.

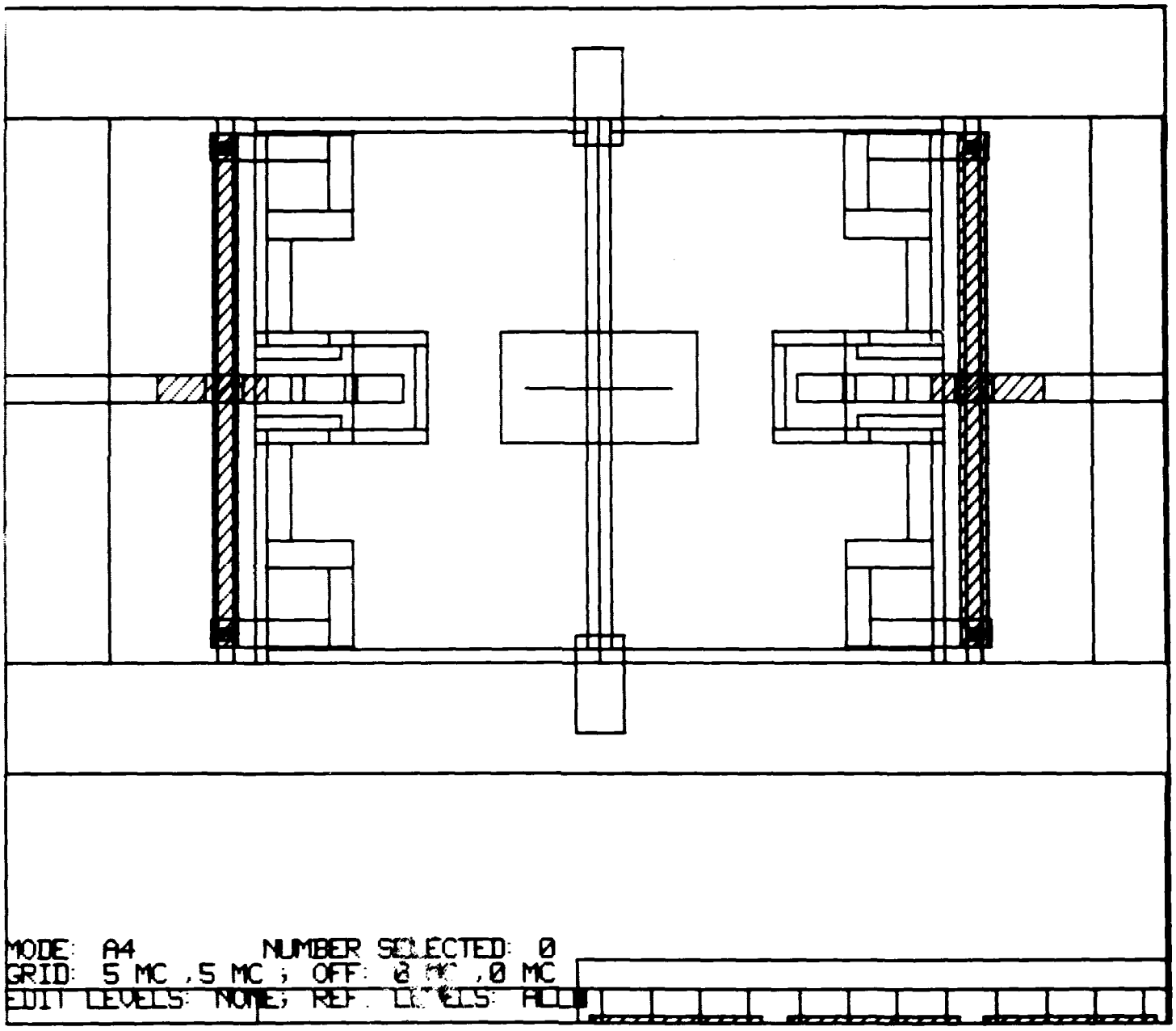

Figure 11d. Composite of the mask artwork for the central section of VCO #4.

R_d is an additional damping resistance placed across the junction to lower the Q below 2. Although a substantial fraction of the microwave power is lost in the additional damping resistances in VCO 3, 4, they provide broad band damping compared to the transformed load of VCO 1, 2 which is well-defined only over the transformer bandwidth near 9GHz. In VCO 2 the inductance was doubled, halving the flux quantum energy, consequently reducing the available output power and the loaded Q.

3.3.2 Fabrication

The composite VCOs, which include the voltage-clamped resistive SQUIDs and matching transformer, were fabricated on 2" silicon wafers using $Nb/Nb_2O_3/PbBi$ junctions, Au resistors, and PbIn interconnection lines. This represents a change from the sapphire substrates originally planned, but permits multiple chip fabrication and easy dicing of the wafer. Also, this method eliminates photoresist problems which occur at the edge of the wafer.

The change from sapphire to silicon substrates produced a problem holding substrates in the vacuum system. Since silicon is more fragile than sapphire, one cannot rigidly clamp the substrate for efficient heat sinking. Vacuum grease is effective at providing efficient heat transfer and mechanical support even for substrates mounted upside down. However, the grease is a potential contaminant for the process which occurs after the vacuum deposition. We have adopted a practice of scraping the grease and cleaning with hot xylene before doing lift-off in acetone. This technique appears manageable although clearly not optimum.

A more common problem was one of multi-layer deposition and processing where good electrical contact is required between layers. Three different vacuum systems were used for this project: an S-Gun sputtering system for Nb deposition, an ion gun system for junction formation, and an e-beam evaporator for other depositions. Only the ion gun system permitted in vacuo cleaning before deposition. The PbBi junction counter-electrode is thermally evaporated in the ion gun system immediately after reactive-ion-oxidation. However, we found significant problems with contacts

when films were deposited in e-beam system. On a temporary basis, we were thermally depositing other metals in the ion gun system, thereby permitting ion cleaning of the surface immediately prior to evaporation. This showed some improvement but was not completely successful, particularly for the alloy films. Also, this multiple use of the ion gun system led to contamination of the system with other materials prior to junction formation.

This problem was addressed more extensively under our IR&D program and we believe it has been resolved successfully. The e-beam system was modified mechanically and electrically to include an rf sputtering stage on which the substrates are mounted. RF sputter cleaning is then performed immediately prior to each new evaporation. Results with this new system are very encouraging. We have fabricated VCO circuits which show satisfactory junctions and connections. Voltage-biasing resistors in the 50-100mΩ range have been fabricated, one or two orders of magnitude larger than desirable. Figure 12 shows photographs of the SQUID section of the four different VCO chips after fabrication.

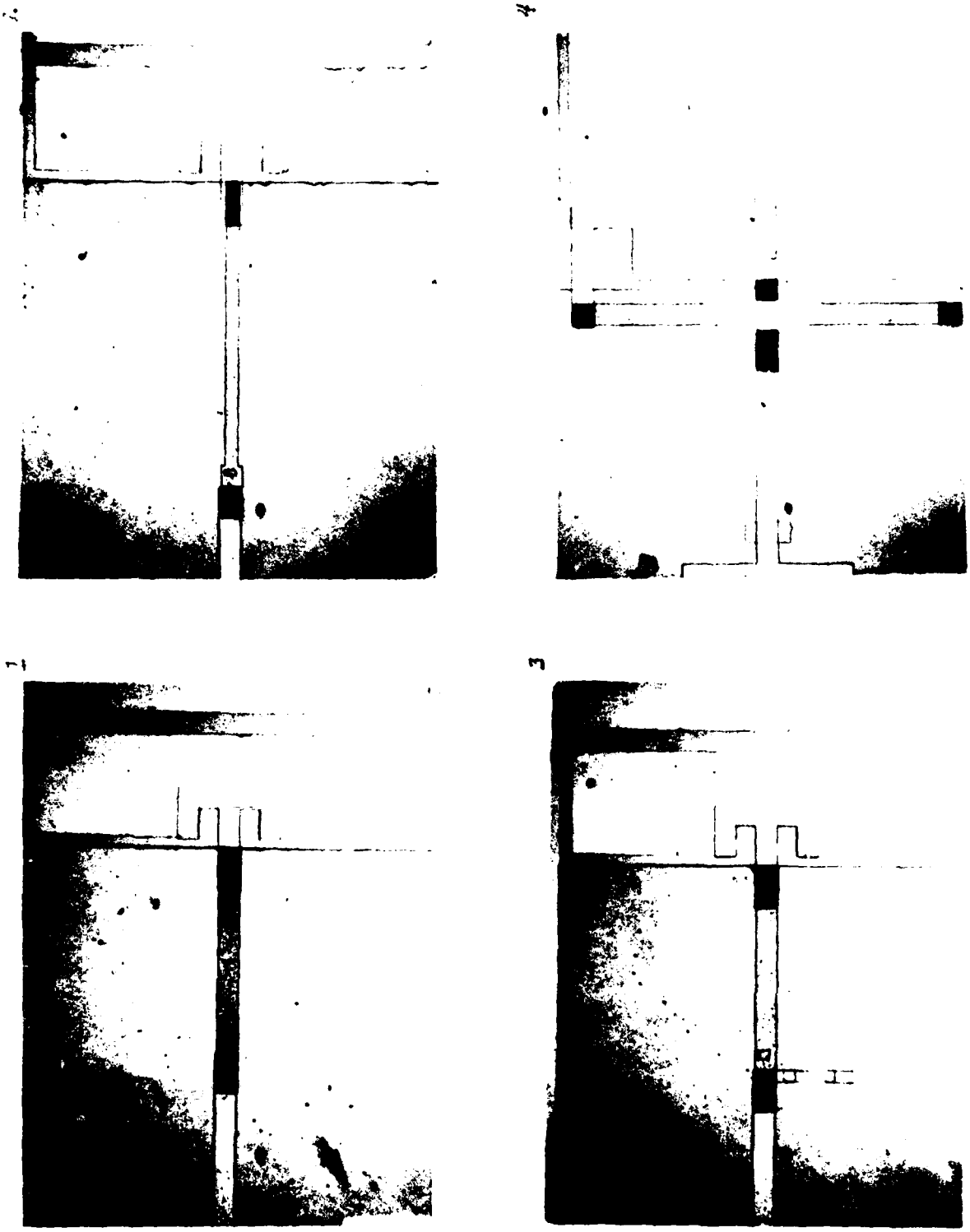

Figure 12. Photographs of the central sections of the four different VCO chips after fabrication.

4. CONCLUSIONS

Measurements show that the SQUID does generate microwave power, but the linewidth is much broader than expected. We believe this is a result of both external noise and internal instabilities of the type identified in 3.2. We are continuing to refine the measurements and SQUID parameters to demonstrate a well-behaved VCO.

SQUID VOLTAGE-CONTROLLED-OSCILLATOR*

A.H. Silver, R.D. Sandell, and J.Z. Wilcox
TRW Space and Technology Group
One Space Park, Redondo Beach, CA 90278

Abstract

We have investigated the SQUID as a voltage-controlled source of microwaves. The low impedance "resistive" SQUID can be a relatively high power (~nW), tunable, and monochromatic source for both on-chip and off-chip applications. Studies of the time-dependent junction phase and the available power spectra as they vary with such device parameters as loaded Q and the SQUID-$\beta=2\pi Li_c/\phi_o$ establish design rules for a well-behaved oscillator. For a VCO $\beta Q<2$; for $\beta Q>2$ degenerate parametric subharmonic oscillations and chaotic instabilities are observed. Power increase is suggested by the use of voltage-clamped dc SQUIDs and arrays.

Introduction

The superconducting voltage-controlled-oscillator (VCO) has potential applications as an integrated, on-chip source for such superconducting devices as analog-to-digital converters (sampling clock), rf SQUID magnetometers (excitation source), parametric amplifiers (pump source), quasiparticle mixers (local oscillator), and intracomputer communications. A source of sufficiently high power can be useful as an agile signal generator. This paper describes the SQUID VCO as the implementation of this source.

The impetus for development of microwave/millimeter wave signal generators in superconducting technology has its origin in the Josephson relations which predict a sinusoidal Josephson current under the application of a dc voltage which is linearly related to the Josephson frequency, $\omega_J=2\pi V/\phi_o$. Unfortunately, problems of impedance and the dynamics of the junction phase have made it difficult to achieve the expected performance.

We argue here that the SQUID and SQUID arrays are the natural forms for a VCO. In order to achieve linear tuning, the source resistance must be small compared to the junction impedance. Such a small resistance connected directly across the junction would short out the Josephson oscillations, greatly reduce the signal voltage across the junction, and no power will be delivered to the load. However, in a resistive SQUID (Fig. 1) the voltage-biasing resistor is isolated from the junction by the SQUID inductance L. Thus, the dc voltage will be developed across the bias resistor, the ac voltage across the inductance, and the total voltage across the junction.

Tunnel junctions generally have lower internal conductance than microbridges, at least below the energy gap, and are desirable junctions to minimize internal losses. The shunt capacitance of the tunnel junction, which is frequently considered a serious shunting impedance, can be effectively parallel-tuned by the SQUID inductance. The load resistance, together with the internal junction resistance, will determine the loaded Q of the VCO.

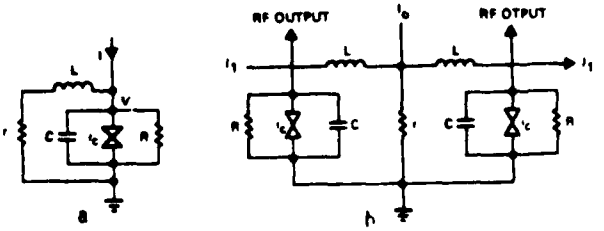

Figure 1. Equivalent circuit of SQUID VCO. (a) Resistive SQUID; (b) Voltage-clamped dc SQUID.

*Supported by the Office of Naval Research, Contract No. N00014-81-C-0615.

Manuscript received November 30, 1982

One expects the instantaneous signal bandwidth to be determined by the Johnson noise across the net (low frequency) resistance as a result of frequency modulation of the oscillator by the thermal voltage fluctuations. This has been predicted and verified for point contact devices[1] as $\delta f=4\pi kTr/\phi_o^2=4.3\times10^{10}rT$ for a biasing resistance r at temperature T. This value is independent of frequency to the extent that the bias current is stable and noise-free.

The stable operating mode of a low $\beta=2\pi Li_c/\phi_o$ SQUID consists of regular flow of quantized flux ϕ_o. The internal circulating power in the SQUID is essentially that of changing quantized flux in the inductance L at the oscillation frequency, $P_{int}=\phi_o^2\omega_J/4\pi L$, while the power delivered to the load resistance is V^2/R where $V=\phi_o\omega_J/2\pi$. Thus, the power in the load is $P_R=P_{int}/\pi Q$ where $Q=R/\omega_J L$. Realistic values of L approximately 10^{-12}H project to $\sim10^{-9}$W of power near 10GHz, with power increasing linearly with frequency at constant Q. This relation for P_R should be valid as Q decreases until the VCO is sufficiently loaded by R to reduce the ac voltage. Fundamental to achieving these power levels is small L and small Q. This requirement leads directly to load resistance values $R=Q\omega_J L$ of the order of $10^{-1}\Omega$ for $Q\sim1$, $L\sim10^{-12}$H, and $f_J\sim10$GHz. Proper impedance matching is clearly necessary for both on-chip and off-chip applications. Coherent arrays of SQUIDs which will increase the total impedance can increase the available power as well as simplify the impedance matching.

Resistive SQUID

We have investigated the voltage-clamped SQUID in two forms: the resistive SQUID (Fig. 1a) and the dual resistive SQUID with common voltage-biasing resistor which we call the voltage-clamped dc SQUID (Fig. 1b). The dynamical response of the SQUID shown in Fig. 1a was simulated numerically to predict the operating characteristics of the SQUID VCO. We envision R to be the load to which power is delivered. This circuit obeys the relation

$$\ddot{\theta}+(\eta_R+\eta_r)\dot{\theta}+(1+\eta_r\eta_R+\beta\cos\theta)\dot{\theta}+\eta_r\beta\sin\theta=\dot{\beta}_I+\eta_r\beta_I \quad (1)$$

where θ is the junction phase, $\eta_R=\sqrt{L/C}/R=Q^{-1}$, $\eta_r=r/\sqrt{L/C}$, $\beta=2\pi Li_c/\phi_o$, $\beta_I=2\pi LI/\phi_o$, and time is measured in $1/\omega_o=\sqrt{LC}$. The voltage across the junction and load resistor R is $V=\dot{\theta}\omega_o\phi_o/2\pi$. The last term on the right hand side of Eq. (1) is approximately the expected Josephson frequency ω_J/ω_o for $I>>i_c$ and is equivalent to a voltage source (rI) in series with r; the actual dc voltage across the junction is somewhat lower than rI and must be determined by either direct measurement or calculation of $\langle\dot{\theta}\rangle$.

The simulations derived $\theta(t)$ and $\dot{\theta}(t)$ for selected values of η_r, η_R, β, and β_I with $\dot{\beta}_I=0$. The results are essentially independent of η_r for all reasonable values of interest and so $\eta_r=10^{-3}$ is used in all calculations reported here. This means that $I=10^3 i_c$ and, hence, $\beta_I=10^3$ at $\omega_J=\omega_o$.

The transient response is dominated by ω_o, Q and ω_J. Figure 2 shows the time evolution of θ and $\dot{\theta}$ for $\beta=1$, $Q=1$ and 5 for selected values of the voltage bias. For $Q=1$, the turn-on transient is short

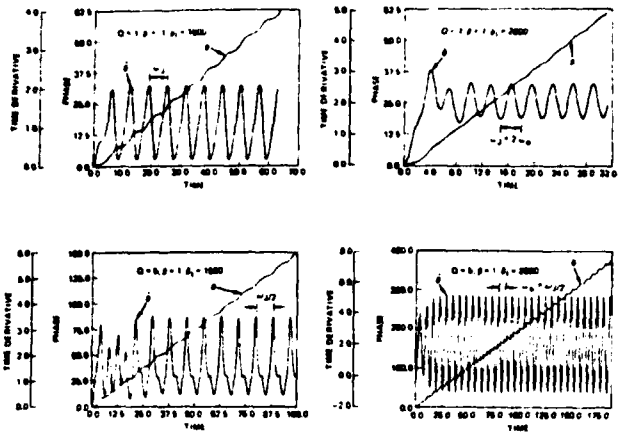

Figure 2. Selected transient response of θ and $\dot{\theta}$ for the resistive SQUID with β=1. Time is in units of ω_o^{-1}.

(approximately Q/ω_o) and associated with shock excitation of the resonant LC circuit, the fundamental frequency of the periodic response is ω_J, and the periodicity in a smoothly stepped θ is 2π. If the Q is raised to 5, the transient response is longer and the resonance frequency becomes further involved with the oscillation. At ω_J/ω_o=1.5 (β_L=1500), there is a strong subharmonic component evident in the time response. At ω_J/ω_o=2 (β_L=2000), the response appears to be totally at $\omega_o=\omega_J/2$, while for Q=1 there was no evident subharmonic response. Generally, for either large β or large Q, the response becomes very complex and even aperiodic. The values required are not 100's, but of the order of 5. Even for smaller values, peculiarities occur somewhere in the spectrum if $\beta Q \geq 2$.

In order to classify and quantify these measurements we have computed the power spectra for selected values of Q and β as a function of β_L. These were computed over 100 periods of the fundamental frequency of the oscillator after a long time interval after turn on, approximately 10^3 cycles. The Fourier amplitudes, including the dc value of $\langle\dot{\theta}\rangle$, were calculated. The zero frequency amplitude was then compared to the fundamental frequency which was first calculated in establishing the time interval for the numerical integration. In general the fundamental frequency is $\langle\dot{\theta}\rangle=\omega_J/n$, except for anharmonic cases for which no fundamental frequency was found. Since the Fourier analysis was performed by a Fourier series no spectra were determined for anharmonic cases.

The power delivered to the load resistance R at any frequency is $P_i=V_i^2/R$ where V_i is the Fourier amplitude of the voltage at that frequency. The value computed numerically is $(\dot{\theta}_i^2/Q)$ which can be converted to physical units according to the relation

$$P_i = \omega_o \phi_o^2 \dot{\theta}_i^2/(2\pi)^2 LQ. \qquad (2)$$

Figure 3 shows the dependence of the power delivered at ω_J for $\omega_J=\omega_o$ as a function of Q for β=1. The power has the expected maximum near Q=3, decreasing at high Q as Q^{-1} and at low Q because of loading of the SQUID. The maximum value of the power is approximately $1.124\ \phi_o^2\omega_o/(2\pi)^2L$. For design values $\omega_o=2\pi\times9\times10^9$ and L=1pH, this corresponds to 12.9nW. However, as we have seen, values of Q>2 lead to some undesirable spectral response. Nevertheless, even for Q=1, the power is not even diminished by a factor of 2 from the peak value.

Figure 4 shows a compilation of the computed powers of the Josephson oscillations as a function of Q for β=1. In the regime Q≤2, the spectra are well

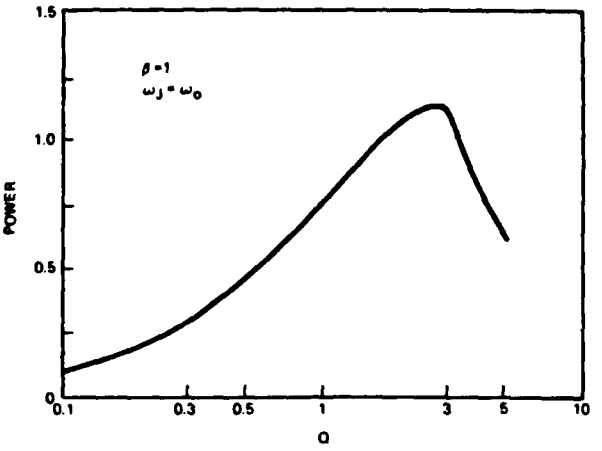

Figure 3. Q-dependence of the power delivered to the load at $\omega_J=\omega_o$ for β=1 in the resistive SQUID. Power is normalized to $[\omega_o\phi_o^2/(2\pi)^2L]$.

behaved except for a subharmonic response at $\omega_J=1.2\omega_o$, Q=2. For Q>2, there is a very strong subharmonic response at $\omega_J=2\omega_o$, and anharmonic response near $\omega_J=1.2\omega_o$. For 2<Q<5, the region near $\omega_J=1.2\omega_o$ exhibits subharmonic behavior which is not plotted.

The strong subharmonic response when $\omega_J=2\omega_o$, which occurs at such modest Q's as 2.5, suggests degenerate parametric oscillations such as those predicted for the SQUID parametric amplifier[2]. This is also suggestive of the period-doubling effects reported to visit nonlinear systems such as Josephson junctions[3]. However, we also observe odd subharmonic responses for Q=5, β=1 which do not fall in the period-doubling class. An example of this is shown in Fig. 5 for Q=5, β=1, and β_L=1100.

These non-period-doubling subharmonics and the nonharmonic response occur in the general vicinity of $\omega_J=1.2\omega_o$ for Q=5, β=1; Levinson[4] has recently predicted odd-subharmonic response as the natural form of the instability in highly undamped Josephson junctions. For simulations which were conducted over a wide range of values of ω_J, the nonharmonic and odd-harmonic response is very localized in ω_J, although we only studied relatively small values of Q. Inspection of $\theta(t)$ suggests that θ spends relatively more time near $(2n+1)\pi$ in this regime, compared to $2n\pi$ for the more well-behaved regime. Since the junction is basically

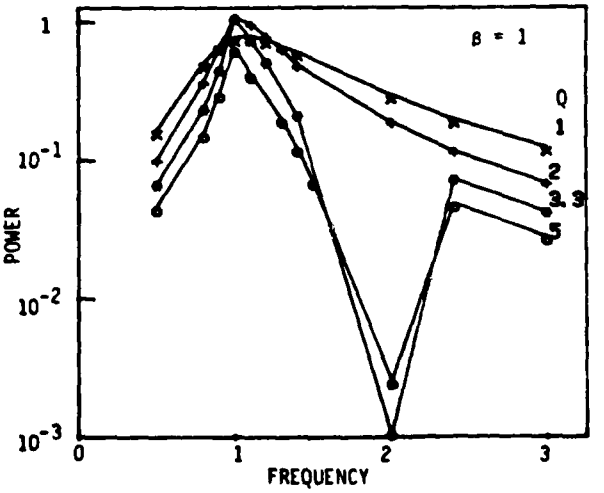

Figure 4. Frequency dependence of the power delivered to the load at ω_J for selected Q-values with β=1 in the resistive SQUID. Power is normalized to $[\omega_o\phi_o^2/(2\pi)^2L]$.

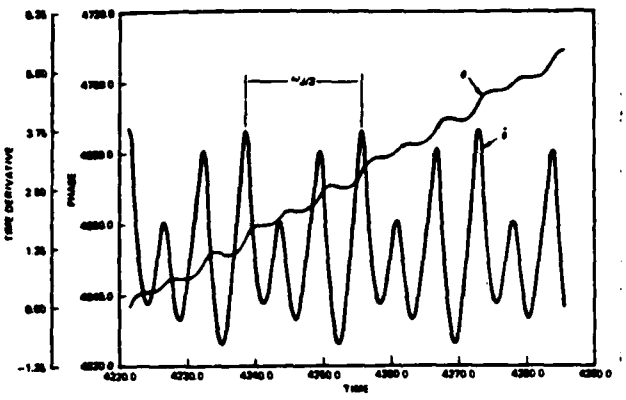

Figure 5. Computed transient response θ and $\dot{\theta}$ for the resistive SQUID with β=1, Q=5, and β_1=1100, corresponding to ω_J=1.1 ω_o. Time is measured in ω_o^{-1}.

unstable for principal values $\pi/2<\theta<-\pi/2$, this may be related to the instability.

The expected effect of increasing β at constant Q=1 is illustrated in the power spectra of Fig. 6. The bracketed symbols are the Josephson frequencies; the symbols connected by straight lines the predicted harmonics. Not all harmonic spectra are shown. Below $\beta=\pi$, all computed points are well behaved with some expected harmonics but no subharmonic response. For $\beta=\pi$, we observe subharmonics as we did for large Q values at β=1. For $\beta>\pi$, the time dependent response becomes even more complex and we have not computed spectral powers. Such β-values would be considered outside the normal range for a SQUID and moves toward the non-SQUID Josephson junction for which this analysis indicates very poor quality VCO.

Voltage-Clamped DC SQUID

The voltage-clamped dc SQUID of Fig. 1b can be recognized as a combination of two identical resistive SQUIDs with a common biasing resistor r. This leads to strong coupling of the two VCO's with identical frequencies but relative phases determined by the field current I_1. Two different modes of the coupled system[6] are essentially a symmetric mode, with the two junctions in parallel, and an antisymmetric mode, with the two junctions in series. Maximum output power and impedance are achieved for the antisymmetric or series mode in which the circulating currents are in the same direction.

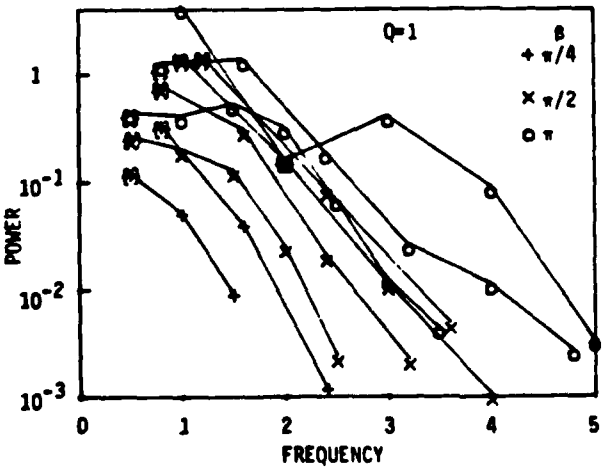

Figure 6. Harmonic spectra for the resistive SQUID with Q=1 and selected β.

We have carried out simulations of the symmetric voltage-clamped dc SQUID shown in Fig. 1b. The new parameters which define the device performance are $\beta_o=2\pi LI_o/\phi_o$, $\beta_1=2\pi LI_1/\phi_o$, $\theta_+=(\theta_R+\theta_L)/2$ and $\theta_-=(\theta_R-\theta_L)/2$. θ_R and θ_L refer to the phases of the right and left hand junctions, respectively, and we have defined β as $2\pi Li_c/\phi_o$, where L is the inductance of one-half of the dc SQUID. In a limited number of simulations with β=1 and β_1=0, the dc SQUID behaves identically to the resistive rf SQUID with $\theta_-=\dot{\theta}_-=0$. The two junctions switch in-phase with one another and the resulting currents in each L add in the small resistance r. However, the voltage across the output (ZL) is identically zero.

For $\beta_1=\pi/2$ and $\beta=1$, the computation shows that $\dot{\theta}_-$ responds at the expected Josephson frequency while $\dot{\theta}_+$ responds at the second harmonic. This frequency doubling is a result of the alternate switching of the two junctions in each Josephson period. We have computed the response at $\beta_1=\pi/2$, $\beta=1$ for a range of Q from 1 to 5; the behavior of θ_- and $\dot{\theta}_-$ is very similar to that observed for θ, $\dot{\theta}$ in the resistive SQUID and will not be reproduced here.

SQUID Array VCO

Arrays of SQUIDs, driven coherently, can achieve further increase in power. Three types of arrays are possible: the longitudinal dc SQUID array, the transverse dc SQUID array, and the resistive SQUID bus. We discuss these briefly. Preliminary descriptions of the longitudinal and transverse dc SQUID arrays were given previously in connection with parametric amplification[7]. Figure 7 shows the simple circuits for both the linear dc SQUID arrays, and for a two-dimensional array which combines the two linear arrays. Analysis of the longitudinal flux-flow array has shown that it is unstable with respect to the flux-flow mode which is the one required for the VCO. As Sandell, et al[7] have shown, this type of array can provide series increase in rf impedance although it requires large dc currents because of its parallel nature at dc. Furthermore, in a tunnel junction implementation as compared with microbridges, narrow linewidths will require small biasing resistors as in the voltage-clamped dc SQUID. The transverse array is recognized as a series array of dc SQUID pairs. It provides increased impedance at both rf and dc, offering a reduction in the direct current required. Again, narrow linewidths will require small biasing resistors. It would be undesirable to fabricate large arrays requiring large numbers of carefully matched small resistors.

A method of avoiding the resistor network and producing a high power array is the resistive SQUID bus as shown in Fig. 7. It is an extension of the voltage-clamped dc SQUID to N resistive SQUIDs with a common voltage-biasing resistor. This could be readily accomplished in a thin film format with a pillbox resistor at the center of a radial array of SQUIDs. These might drive a coaxial line to an off-chip load.

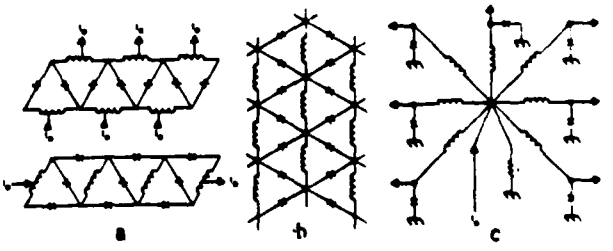

Figure 7. Schematic diagrams of SQUID arrays. (a) Longitudinal (upper) and transverse (lower) flux-flow arrays; (b) Two dimensional array; (c) SQUID bus.

On-chip, the bus can be used to drive many different loads which require coherent input, as in clocking a shift register or driving an array of mixers. If one supplies internal phase shifts of π between adjacent elements (as in the dc SQUID), then one can supply alternate out-of-phase signals. In either case, coherence is guaranteed by the common bias resistor and superconducting phase coherence.

Summary

The SQUID is the natural form for signal generation via the Josephson effect. While the bare Josephson junction suffers from both chaotic instabilities and low impedance, its incorporation in a low β, low Q SQUID tunes out the junction capacitance and controls the instability by directly harnessing the periodic nature of the junction phase to the quantum periodicity of the SQUID magnetic flux. This results in an efficient conversion of the Josephson energy to the circulating current in the SQUID inductance and, hence, to external circuitry. The power is maximized by minimizing the inductance, although at further reduction in source impedance. This last problem is alleviated by forming a priori coherent, stable arrays of SQUIDs to increase both the total power and impedance. Such arrays have the voltage-clamped dc SQUID as the basic cell. The design presented makes minimum demands on both lithography and Josephson current density.

Several experimental results have been reported in recent years which pertain to this device. The group at SUNY have studied microbridge VCO's, including pairs and arrays. The most successful results were in the dc SQUID-like arrays[7] reminiscent of Fig. 7a, although the SQUID inductances were very large compared to the values suggested here. Calander and Zappe[8] proposed using a dc SQUID as a tunable oscillator for intracomputer communication in a Josephson processor. They predicted $\sim 1\mu W$ of power at 500 GHz. Tuckerman[9] demonstrated this concept by connecting a dc SQUID transmitter with another dc SQUID receiver by a superconducting microstripline. The transmitted microwave signals were readily detected. Calendar, et al[10] demonstrated a resistive SQUID VCO incidentally to their self-pumped Josephson parametric amplifier. Using a SQUID with $\beta=2$, $L=3pH$, $r=3\times10^{-2}\Omega$, and a 1Ω matching transformer, they observed 0.15nW at 10.4 GHz with a bandwidth of 150 MHz. This linewidth is much greater than the thermal-noise-limited value, 5 MHz, and is reportedly broadened by noise in the bias current. Assuming that the average power is diminished by the same factor as the line broadening, one could have expected as much as 4.5nW, in excellent agreement with the predictions of the model.

References

1. A.H. Silver, J.E. Zimmerman, and R.A. Kamper, "Contribution of Thermal Noise to the Linewidth of Josephson Radiation from Superconducting Point Contacts," Appl. Phys. Lett. 11, pp. 209-211 (1967).
2. A.H. Silver, D.C. Pridmore-Brown, R.D. Sandell, and J.P. Hurrell, "Parametric Properties of SQUID Lattice Arrays," IEEE Trans. Magn. MAG-17, pp.412-415 (1981).
3. R.L. Kautz, "The ac Josephson Effect in Hysteratic Junctions: Range and Stability of Phase Lock," J. Appl. Phys. 52, pp. 3528-3541 (1981); "Chaotic States of rf-Biased Josephson Junctions," J. Appl. Phys. 52, pp. 6241-6246 (1981).
4. M.T. Levinsen, "Even and Odd Subharmonic Frequencies and Chaos in Josephson Junctions: Impact on Parametric Amplifiers?," J. Appl. Phys. 53, pp. 4294-4299 (1982).
5. J.E. Zimmerman and A.H. Silver, "Coherent Radiation From High-Order Quantum Transitions in Small-Area Superconducting Contacts," Phys. Rev. Lett. 19, pp. 14-16 (1967).
6. A.H. Silver and J.E. Zimmerman, "Coupled Superconducting Quantum Oscillators," Phys. Rev. 158, pp. 423-425 (1967).
7. R.D. Sandell, C. Varmazis, A.K. Jain, and J.E. Lukens, "Flux Modulated Coherent Radiation from Arrays of Josephson Microbridges Coupled by Superconducting Loops," IEEE Trans. Magn. MAG-15, pp. 462-464 (1979).
8. N. Calander and H.H. Zappe, "Components for a Josephson Intracomputer Communication System," J. Appl. Phys. 50, pp. 3768-3769 (1979).
9. D.B. Tukerman, "Digital Frequency-Division Multiplexing Using Josephson Junctions," Thesis, MIT (1980).
10. N. Calander, T. Claeson, and S. Rudner, "Shunted Josephson Tunnel Junctions: High Frequency, Self-Pumped Low Noise Amplifiers," J. Appl. Phys. 53, pp. 5093-5103 (1982).

APPENDIX B

Printout of the computed characteristics of the resistive SQUID VCO. The first line shows the run number, β, Q, β_l, computed fundamental frequency, and subharmonic number relative to the Josephson frequency; the second line is the computed spectral power for the first seven harmonics of the fundamental frequency. Where the frequency and harmonic number are reported as zero, the oscillator is anharmonic.

Run#	β	Q	β_l	ω/ω_0	Subharmonic#		
P_1	P_2	P_3	P_4	P_5	P_6	P_7	
1	0.78	1.00	500	4.993E-01	1		
1.215E-01	5.192E-02	9.052E-03	6.037E-04	4.405E-05	4.121E-06	3.816E-07	
2	0.78	1.00	800	7.989E-01	1		
3.369E-01	4.023E-02	1.706E-03	5.912E-05	2.401E-06	1.111E-07	5.115E-09	
3	0.78	1.00	1000	9.987E-01	1		
5.172E-01	2.063E-02	5.123E-04	1.546E-05	4.701E-07	1.446E-08	4.479E-10	
4	0.78	1.00	1200	1.199E 00	1		
4.861E-01	9.236E-03	1.597E-04	2.920E-06	5.484E-08	1.019E-09	1.917E-11	
5	0.78	1.00	2000	1.998E 00	1		
1.885E-01	4.690E-04	1.231E-06	3.279E 09	8.769E-12	2.344E-14	5.812E-17	
6	1.57	1.00	500	4.989E-01	1		
2.686E-01	2.043E-01	1.304E-01	2.566E-02	2.433E-03	6.043E-04	1.489E-04	
7	1.57	1.00	800	7.985E-01	1		
7.978E-01	3.118E-01	2.104E-02	2.274E-03	3.008E-04	3.683E-05	4.391E-06	
8	1.57	1.00	1000	9.982E-01	1		
1.476E 00	1.644E-01	1.150E-02	1.064E-03	9.289E-05	8.231E-06	7.360E-07	
9	1.57	1.00	1200	1.198E 00	1		
1.500E 00	8.592E-02	4.932E-03	2.864E-04	1.682E-05	9.952E-07	5.900E-08	
10	1.57	1.00	2000	1.998E 00	1		
6.933E-01	6.667E-03	6.659E-05	6.709E-07	6.703E-09	6.850E-11	6.794E-13	
11	3.14	1.00	500	4.977E-01	1		
4.494E-01	4.154E-01	5.263E-01	3.286E-01	6.939E-02	1.259E-02	4.442E-03	
12	3.14	1.00	800	7.974E-01	1		
1.273E 00	1.396E 00	1.910E-01	2.640E-02	1.132E-02	2.722E-03	6.296E-04	
13	3.14	1.00	1000	9.970E-01	1		

Copy available to DTIC does not permit fully legible reproduction

```
3.309E 00  5.415E-01  1.225E-01  2.301E-02  4.516E-03  8.823E-04  1.723E-04

14      3.14      1.00     1200       0.000E 00          0
0.000E 00  0.000E 00  0.000E 00  0.000E 00  0.000E 00  0.000E 00  0.000E 00

15      3.14      1.00     2000       9.984E-01          2
4.324E 00  1.621E-01  4.091E-01  8.964E-02  2.360E-03  1.999E-03  9.504E-04

16      1.00      0.10     1000       9.900E-01          1
9.948E-02  2.472E-04  5.929E-07  1.516E-09  1.097E-11  4.057E-12  3.435E-12

17      1.00      0.25      500       4.978E-01          1
1.950E-01  1.115E-02  5.591E-04  2.694E-05  1.422E-06  1.172E-07  2.789E-08

18      1.00      0.25     1000       9.957E-01          1
2.428E-01  3.274E-03  3.636E-05  3.835E-07  7.727E-09  1.178E-09  7.541E-10

19      1.00      0.25     2000       1.992E 00          1
2.185E-01  4.641E-04  9.824E-07  2.314E-08  1.016E-08  7.187E-09  5.416E-09

20      1.00      0.25     3000       2.988E 00          1
1.734E-01  9.857E-05  6.609E-08  2.313E-09  1.207E-09  9.153E-10  6.811E-10

21      1.00      0.30     1000       9.963E-01          1
2.881E-01  5.249E-03  7.385E-05  9.814E-07  1.934E-08  1.904E-09  9.791E-10

22      1.00      0.50     1000       9.974E-01          1
4.555E-01  1.690E-02  4.041E-04  1.040E-05  4.830E-07  8.373E-08  4.168E-08

23      1.00      1.00      500       4.992E-01          1
1.660E-01  9.371E-02  2.691E-02  2.561E-03  2.436E-01  3.104E-05  4.096E-06

24      1.00      1.00      800       7.998E-01          1
5.030E-01  8.673E-02  3.570E-03  2.270E-04  1.510E-05  1.013E-06  6.715E-08

25      1.00      1.00      900       8.987E-01          1
6.640E-01  6.425E-02  2.416E-03  1.367E-04  7.497E-06  4.143E-07  2.311E-08

26      1.00      1.00     1000       9.986E-01          1
7.694E-01  4.550E-02  1.679E-03  7.656E-05  3.474E-06  1.593E-07  7.367E-09

27      1.00      1.00     1100       1.099E 00          1
7.857E-01  3.149E-02  1.029E-03  3.704E-05  1.350E-06  4.969E-08  1.837E-09

28      1.00      1.00     1200       1.198E 00          1
7.423E-01  2.146E-02  5.723E-04  1.607E-05  4.583E-07  1.316E-08  3.791E-10

29      1.00      1.00     1403       1.398E 00          1
6.024E-01  9.828E-03  1.615E-04  2.723E-06  4.646E-08  7.962E-10  1.367E-11
```

```
30      1.00      1.00     2000      1.998E 00          1
2.966E-01  1.202E-03  5.073E-06  2.1[illegible]E-08  9.276E-11  3.937E-13  1.471E-15

31      1.00      1.00     2400      2.398E 00          1
1.992E-01  3.882E-04  7.841E-07  1.597E-09  3.27[illegible]E-12  [illegible].205E-15  4.827E-17

32      1.00      1.00     3000      2.997E 00          1
1.226E-01  9.711E-05  7.909E-08  6.527E-11  6.371E-14  5.032E-12  1.659E-16

33      1.00      1.50      500      4.994E-01          1
1.248E-01  1.117E-01  4.801E-02  3.853E-03  3.287E-04  5.348E-05  7.592E-06

34      1.00      1.50      800      7.991E-01          1
4.447E-01  1.182E-01  3.07[illegible]E-03  2.755E-04  2.[illegible]E-05  1.733E-06  1.266E-07

35      1.00      1.50      900      8.990E-01          1
7.093E-01  8.340E-02  2.555E-03  2.120E-04  1.432E-05  9.526E-07  6.719E-08

36      1.00      1.50     1000      9.988E-01          1
9.642E-01  5.370E-02  2.812E-03  1.723E-04  1.074E-05  6.825E-07  4.350E-08

37      1.00      1.50     1100      1.099E 00          1
9.503E-01  3.575E-02  1.[illegible]E-03  8.927E-05  4.[illegible]E-06  2.373E-07  1.228E-08

38      1.00      1.50     1200      1.199E 00          1
8.248E-01  2.367E-02  9.123E-04  3.468E-05  1.[illegible]E-06  5.289E-08  2.069E-09

39      1.00      1.50     1300      1.299E 00          1
6.971E-01  1.535E-02  4.[illegible]E-04  1.259E-05  3.664E-07  1.068E-08  3.107E-10

40      1.00      1.50     1400      1.399E 00          1
5.862E-01  9.923E-03  2.119E-04  4.[illegible]E-06  [illegible].944E-08  2.167E-09  4.719E-11

41      1.00      1.50     2000      1.999E 00          1
2.354E-01  9.852E-04  4.683E-06  2.248E-08  1.075E-10  4.840E-13  1.175E-15

42      1.00      1.50     2400      2.398E 00          1
1.490E-01  2.970E-04  6.[illegible]E-07  1.426E-09  3.[illegible]E-12  6.130E-15  3.675E-19

43      1.00      1.50     3000      2.998E 00          1
8.759E-02  7.039E-05  6.001E-08  5.131E-11  4.[illegible]E-14  6.238E-18  7.092E-18

44      1.00      1.75     2000      1.999E 00          1
2.102E-01  8.858E-04  4.332E-06  2.140E-08  1.057E-10  5.150E-13  2.137E-15

45      1.00      2.00      500      4.995E-01          1
1.007E-01  1.137E-01  6.[illegible]E-02  4.135E-03  3.[illegible]E 04  6.442E-05  8.002E-06

46      1.00      2.00      800      7.993E-01          1
3.669E-01  1.270E-01  2.032E-03  2.489E-04  1.[illegible]F 05  1.[illegible]E-06  1.188E-07
```

47 1.00 2.00 900 8.991E-01 1
6.487E-01 8.875E-02 1.899E-03 2.007E-04 1.490E-05 9.597E-07 7.628E-08

48 1.00 2.00 1000 9.989E-01 1
1.071E 00 4.892E-02 3.798E-03 2.529E-04 1.897E-05 1.479E-06 1.119E-07

49 1.00 2.00 1100 1.099E 00 1
9.621E-01 3.313E-02 2.212E-03 1.293E-04 7.967E-06 4.914E-07 3.027E-08

50 1.00 2.00 1200 1.199E 00 1
7.811E-01 2.195E-02 1.013E-03 4.492E-05 2.031E-06 9.177E-08 4.138E-09

51 1.00 2.00 1300 6.495E-01 2
2.677E-09 6.342E-01 3.706E-10 1.399E-02 3.530E-11 4.606E-04 2.671E-12

52 1.00 2.00 1400 6.996E-01 2
4.641E-02 4.846E-01 5.459E-03 7.638E-03 3.530E-04 1.648E-04 1.531E-05

53 1.00 2.00 2000 9.995E-01 2
1.352E-06 1.890E-01 5.227E-08 7.999E-04 8.518E-10 3.984E-06 2.237E-11

54 1.00 2.00 2400 2.399E 00 1
1.167E-01 2.345E-04 5.274E-07 1.195E-09 2.712E-12 6.214E-15 2.180E-17

55 1.00 2.00 3000 2.998E 00 1
6.737E-02 5.441E-05 4.472E-07 4.097E-11 3.013E-14 3.603E-19 1.323E-17

56 1.00 2.25 2000 9.995E-01 2
4.572E-01 1.021E-01 1.298E-02 3.144E-04 9.165E-05 7.955E-06 5.421E-07

57 1.00 2.50 500 4.995E-01 1
8.473E-02 1.088E-01 7.085E-02 3.806E-03 2.721E-04 6.833E-05 6.539E-06

58 1.00 2.50 800 7.994E-01 1
3.045E-01 1.243E-01 1.364E-02 2.122E-04 1.404E-05 1.619E-06 9.149E-08

59 1.00 2.50 900 8.993E-01 1
5.638E-01 8.772E-02 1.292E-03 1.607E-04 1.300E-05 7.306E-07 6.398E-08

60 1.00 2.50 1000 9.990E-01 1
1.124E 00 3.991E-02 4.659E-03 3.138E-04 2.681E-05 2.404E-06 2.038E-07

61 1.00 2.50 1100 1.099E 00 1
8.890E-01 2.963E-02 2.219E-03 1.459E-04 9.807E-06 6.609E-07 4.448E-08

62 1.00 2.50 1200 5.996E-01 2
1.442E-02 6.861E-01 1.783E-03 1.962E-02 2.928E-04 9.096E-04 2.558E-05

```
63      1.00      2.50     1300      6.456E-01          2
9.231E-02  4.762E-01  1.040E-02  9.082E-03  9.778E-04  2.832E-04  5.693E-05

64      1.00      2.50     1400      6.996E-01          2
1.744E-01  3.254E-01  1.594E-02  4.636E-03  9.265E-04  1.224E-04  3.601E-05

65      1.00      2.50     1500      9.995E-01          2
9.428E-01  4.213E-02  1.816E-02  1.428E-03  8.232E-05  1.830E-05  2.253E-06

66      1.00      2.50     2400      2.999E 00          1
9.531E-02  1.922E-04  4.384E-07  1.008E-09  2.323E-12  5.899E-15  4.805E-17

67      1.00      2.50     3000      2.999E 00          1
5.454E-02  4.415E-05  3.859E-08  3.390E-11  2.374E-14  2.681E-17  2.059E-18

68      1.00      3.00     1000      9.990E-01          1
1.124E 00  3.054E-02  5.238E-03  4.045E-04  3.459E-05  3.788E-06  3.594E-07

69      1.00      3.00     1100      1.099E 00          1
7.966E-01  2.650E-02  2.059E-03  1.445E-04  1.028E-05  7.267E-07  5.126E-08

70      1.00      3.00     1200      5.997E-01          2
5.985E-02  5.636E-01  5.706E-03  1.402E-02  1.006E-03  6.915E-04  8.586E-05

71      1.00      3.00     1300      6.497E-01          2
1.313E-01  3.738E-01  1.213E-02  7.033E 03  1.163E-03  2.498E-04  6.650E-05

72      1.00      3.00     1400      6.997E-01          2
2.067E-01  2.443E-01  1.615E-02  3.879E-03  9.236E-04  1.321E-04  3.637E-05

73      1.00      3.00     2000      9.995E-01          2
1.496E 00  5.686E-02  1.455E-02  3.404E-03  2.85.E-04  2.020E-05  4.354E-06

74      1.00      3.00     2400      2.999E 00          1
8.033E-02  1.623E-04  3.731E-07  8.635E-10  1.992E-12  4.962E-15  6.964E-18

75      1.00      3.00     3000      2.999E 00          1
4.575E-02  3.707E-05  3.056E-08  2.889E-11  2.876E-14  1.451E-16  3.204E-17

76      1.00      3.30      500      4.996E-01          1
6.735E-02  9.665E-02  7.223E-02  2.889E-03  1.938E-04  6.801E-05  3.832E-06

77      1.00      3.30      800      7.995E-01          1
2.356E-01  1.121E-01  8.004E-04  1.647E-04  3.311E 06  1.349E-06  5.520E-08

78      1.00      3.30      900      8.994E-01          1
4.496E-01  8.035E-02  7.290E-04  1.060E-04  1.016E-05  4.426E-06  4.315E-08

79      1.00      3.30     1000      9.991E-01          1
1.054E 00  3.537E-02  4.534E-03  2.695E-04  2.169E-05  2.356E-06  1.919E-07
```

```
80      1.00      3.30     1100      5.497E-01          2
6.210E-03  7.405E-01  3.157E-04  2.422E-02  1.572E-04  1.912E-03  1.879E-05

81      1.00      3.30     1200      5.997E-01          2
7.361E-02  5.091E-01  6.169E-03  1.237E-02  1.141E-03  6.292E-04  9.703E-05

82      1.00      3.30     1400      6.997E-01          2
2.102E-01  2.122E-01  1.534E-02  3.628E-03  8.794E-04  1.344E-04  3.533E-05

83      1.00      3.30     2000      9.995E-01          2
1.677E 00  1.052E-03  1.132E-02  3.918E-03  4.523E-04  3.031E-05  4.184E-06

84      1.00      3.30     2400      2.399E 00          1
7.336E-02  1.483E-04  3.421E-07  7.950E-10  1.688E-12  5.055E-15  6.074E-17

85      1.00      3.30     3000      2.999E 00          1
4.170E-02  3.380E-05  2.979E-08  2.636E-11  2.497E-14  7.334E-17  1.121E-17

86      1.00      5.00      500      4.997E-01          1
4.627E-02  7.318E-02  6.408E-02  1.410E-03  1.020E-04  5.983E-05  1.268E-06

87      1.00      5.00      800      7.997E-01          1
1.570E-01  8.590E-02  3.742E-04  1.079E-04  4.070E-05  9.593E-07  2.060E-08

88      1.00      5.00      900      8.996E-01          1
3.055E-01  6.245E-02  3.071E-04  5.070E-05  6.564E-06  1.667E-07  2.162E-08

89      1.00      5.00     1000      9.995E-01          1
6.492E-01  4.338E-02  1.775E-03  8.636E-05  7.057E-06  6.227E-07  3.834E-08

90      1.00      5.00     1100      1.833E-01          6
2.704E-07  9.691E-03  2.107E-06  1.322E-01  1.432E-04  4.218E-01  3.834E-07

91      1.00      5.00     1100      3.666E-01          3
9.680E-03  1.322E-01  4.218E-01  3.160E-03  3.702E-03  1.059E-02  1.191E-04

92      1.00      5.00     1150      0.000E 00          0
0.000E 00  0.000E 00  0.000E 00  0.000E 00  0.000E 00  0.000E 00  0.000E 00

93      1.00      5.00     1200      0.000E 00          0
0.000E 00  0.000E 00  0.000E 00  0.000E 00  0.000E 00  0.000E 00  0.000E 00

94      1.00      5.00     1250      0.000E 00          0
0.000E 00  0.000E 00  0.000E 00  0.000E 00  0.000E 00  0.000E 00  0.000E 00

95      1.00      5.00     1300      1.624E-01          8
9.229E-07  1.800E-04  1.934E-05  1.023E-01  8.947E-05  3.470E-02  4.757E-06
```

```
 96      1.00      5.00     1300      3.250E-01          4
8.010E-04  1.020E-01  3.457E-02  1.998E-01  7.103E-04  6.746E-03  1.336E-03

 97      1.00      5.00     1400      3.499E-01          4
5.351E-05  1.599E-01  2.534E-02  1.228E-01  4.912E-04  9.375E-03  7.533E-04

 98      1.00      5.00     1500      7.496E-01          2
2.426E-01  7.130E-02  1.192E-02  2.003E-03  4.446E-04  7.917E-05  1.543E-05

 99      1.00      5.00     2000      9.996E-01          2
1.840E 00  2.588E-03  2.490E-03  3.572E-03  8.171E-04  1.015E-04  7.962E-06

100      1.00      5.00     2400      2.400E 00          1
4.901E-02  9.928E-05  2.308E-07  5.408E-10  1.276E-12  9.333E-15  3.026E-17

101      1.00      5.00     3000      2.999E 00          1
2.771E-02  2.249E-05  1.986E-08  1.753E-11  1.382E-14  2.648E-18  1.405E-17
```

Copy available to DTIC does not permit fully legible reproduction

DISTRIBUTION LIST
FOR
TECHNICAL REPORTS

CONTRACT NO. N00014-81-C-0615

Scientific Officer 1
Director, Electronic & Solid State Sciences Program
Physical Sciences Division
Office of Naval research
800 North Quincy Street
Arlington, VA 22217
Attn: Mr. Edgar A. Edelsack
Ref: Contract N00014-81-C-0615

Administrative Contracting Officer 1
Office of Naval Research
800 North Quincy Street
Arlington, VA 22217
Ref: Contract N00014-81-C-0615

Director 6
Naval Research Laboratory
Code 2627
Washington, DC 20375

Defense Technical Information Center 12
Building 5
Cameron Station
Alexandria, VA 22314

Office of Naval Research 1
Western Regional Office
1030 E. Green Street
Pasadena, CA 91106

Dr. Martin Nisenoff, Code 6854 1
Naval Research Laboratory
4555 Overlook Ave., SW
Washington, DC 20375

Dr. Fernand D. Bedard 1
Department of Defense
R03
Fort Meade, MD 20755

Dr. Nancy K. Welker 1
Laboratory for Physical Sciences
4928 College Avenue
College Park, MD 20740

Dr. Kenneth Davis, Code 6855 1
Naval Research Laboratory
4555 Overlook Avenue, SW
Washington, DC 20375

Max N. Yoder, Code 414 — 1
Office of Naval Research
800 North Quincy Street
Arlington, VA 22217

Dr. James E. Zimmerman — 1
Mail Stop 2137
National Bureau of Standards
Boulder, CO 80302

Dr. Clark A. Hamilton — 1
Room 2137
National Bureau of Standards
325 S. Broadway
Boulder, CO 80303

Mr. Ernest Stern — 1
MIT-P-327
Lincoln Laboratory
P. O. Box 73
Lexington, MA 02173

Dr. Ted Van Duzer — 1
Dept. of Electrical Engineering and Computer Science
University of California
Berkeley, CA 94720

TRW Documents Section — 1
Technical Information Center (TIC)
Building S, Room 1930
One Space Park
Redondo Beach, CA 90278


FILME
5-8